

Review

Plasmonic Nanoparticles as Optical Sensing Probes for the Detection of Alzheimer's Disease

María Paz Oyarzún ^{1,2} , Andreas Tapia-Arellano ^{1,2}, Pablo Cabrera ^{1,2}, Pedro Jara-Guajardo ^{1,2}
and Marcelo J. Kogan ^{1,2,*} 

- ¹ Departamento de Química Farmacológica y Toxicológica, Facultad de Ciencias Químicas y Farmacéuticas, Universidad de Chile, Dr. Carlos Lorca Tobar 964, Independencia, 8380000 Santiago, Chile; maria.oyarzunm@usach.cl (M.P.O.); atare_28@ciq.uchile.cl (A.T.-A.); pablo.cabrera@ug.uchile.cl (P.C.); pedro.jara@ug.uchile.cl (P.J.-G.)
- ² Advanced Center for Chronic Diseases (ACCDIS), Sergio Livingstone #1007, Independencia, 8380492 Santiago, Chile
- * Correspondence: mkogan@ciq.uchile.cl

Abstract: Alzheimer's disease (AD), considered a common type of dementia, is mainly characterized by a progressive loss of memory and cognitive functions. Although its cause is multifactorial, it has been associated with the accumulation of toxic aggregates of the amyloid- β peptide ($A\beta$) and neurofibrillary tangles (NFTs) of tau protein. At present, the development of highly sensitive, high cost-effective, and non-invasive diagnostic tools for AD remains a challenge. In the last decades, nanomaterials have emerged as an interesting and useful tool in nanomedicine for diagnostics and therapy. In particular, plasmonic nanoparticles are well-known to display unique optical properties derived from their localized surface plasmon resonance (LSPR), allowing their use as transducers in various sensing configurations and enhancing detection sensitivity. Herein, this review focuses on current advances in in vitro sensing techniques such as Surface-enhanced Raman scattering (SERS), Surface-enhanced fluorescence (SEF), colorimetric, and LSPR using plasmonic nanoparticles for improving the sensitivity in the detection of main biomarkers related to AD in body fluids. Additionally, we refer to the use of plasmonic nanoparticles for in vivo imaging studies in AD.

Keywords: nanoparticle based-plasmonic sensors; Alzheimer's disease; AD biomarkers; kinetics of aggregation; amyloid- β peptide; tau protein; SERS detection; fluorescence detection; colorimetric detection; LSPR detection; in vivo imaging detection



Citation: Oyarzún, M.P.; Tapia-Arellano, A.; Cabrera, P.; Jara-Guajardo, P.; Kogan, M.J. Plasmonic Nanoparticles as Optical Sensing Probes for the Detection of Alzheimer's Disease. *Sensors* **2021**, *21*, 2067. <https://doi.org/10.3390/s21062067>

Academic Editor: Abel Santos

Received: 19 January 2021

Accepted: 11 March 2021

Published: 16 March 2021

Publisher's Note: MDPI stays neutral with regard to jurisdictional claims in published maps and institutional affiliations.



Copyright: © 2021 by the authors. Licensee MDPI, Basel, Switzerland. This article is an open access article distributed under the terms and conditions of the Creative Commons Attribution (CC BY) license (<https://creativecommons.org/licenses/by/4.0/>).

1. Introduction

Alzheimer's disease (AD) is a neurodegenerative disease (NDD) and is the most common kind of dementia, with a typical clinical presentation characterized by loss of memory and cognitive impairment. AD involves different processes that finally lead to both synaptic and neuronal loss in brain regions such as the cerebral cortex and subcortical area, triggering cognitive impairment, memory loss, brain dysfunction, and behavioral disorders [1,2].

The accumulation and aggregation of the amyloid- β peptide ($A\beta$) as extracellular deposits and the formation of intraneuronal aggregates of hyperphosphorylated tau protein (P-tau) as neurofibrillary tangles (NFTs) in the brain, associated by inflammation and oxidative stress processes [3] have been described as the pathological hallmarks of AD. In addition, more recently several studies have suggested that soluble $A\beta$ oligomers ($A\beta$ Os) are the most toxic species formed, leading to a synaptic dysfunction [4–7].

Since these $A\beta$ species have been identified according to their direct participation in the development of AD, various biomarkers could be useful to detect AD in the pre-dementia phase [8] and to start an effective treatment to prevent further deleterious damage on the brain and neuronal loss. The core cerebrospinal fluid (CSF) biomarkers: total tau

(T-tau), phosphorylated tau (P-tau) and the 42-amino acid form of A β (A β_{1-42}) are the most frequently used as AD-related biomarkers [9,10]. Thus, low concentration levels of A β_{1-42} can be detected in CSF at the onset of the disease, whereas concentrations of T-tau and P-tau are increased and are detected in long-term courses [8,11]. On the other hand, an increased A β_{1-42} /A β_{1-40} ratio in CSF indicates increased levels of A β_{1-42} [12], which is more prone to aggregate than A β_{1-40} . A β_{1-42} has been related to increased neurotoxicity of A β and is considered a reliable index due to its high diagnostic accuracy [10].

Moreover, some studies have focused on genetic components that can be considered as risk factors. In fact, the presence of high levels of apolipoprotein E4 allele (ApoE4) has been considered as a major genetic risk factor of AD, whereas high levels of apolipoprotein E2 allele (ApoE2) would exert a protective role [13,14].

In this context, the development of analytical devices for rapid, sensitive, reliable, and low-cost methods for the simultaneous detection of various AD biomarkers in primary stages of the disease could contribute to improve understanding of the molecular mechanisms underlying the pathophysiology of this disease [3].

In particular, the fabrication of sensors for the detection of biological analytes with high sensitivity and selectivity has significantly increased in the last decade. In this field, nanomaterials have become an interesting and useful tool due to their versatile uses, such as the ability to immobilize biorecognition molecules on their surface, the high surface-area-to-volume ratio, or the capability to amplify signals, which could facilitate recognizing and sensing molecules of biological interest [3,15]. Among these nanomaterials, “plasmonic metal nanoparticles” (including gold, silver, platinum, etc.) are those that support a localized surface plasmon resonance (LSPR) phenomena, allowing them to absorb and scatter the light in different ways. These interesting and useful properties making them excellent candidates for broad applications in the nanomedicine field, as diagnostics (sensing), imaging, or therapeutics (therapy agents) [16].

The present review focuses on the advances made during the last decade (2010–2020) in the development and application of plasmonic nanoparticles in optical sensors for *in vitro* detection of main AD biomarkers in artificial and real samples. In addition, we refer to some studies of the application of these nanoparticles for imaging in *in vivo* diagnosis, as illustrated in Figure 1. Finally, this review brings into focus future perspectives of the biosensing of AD.

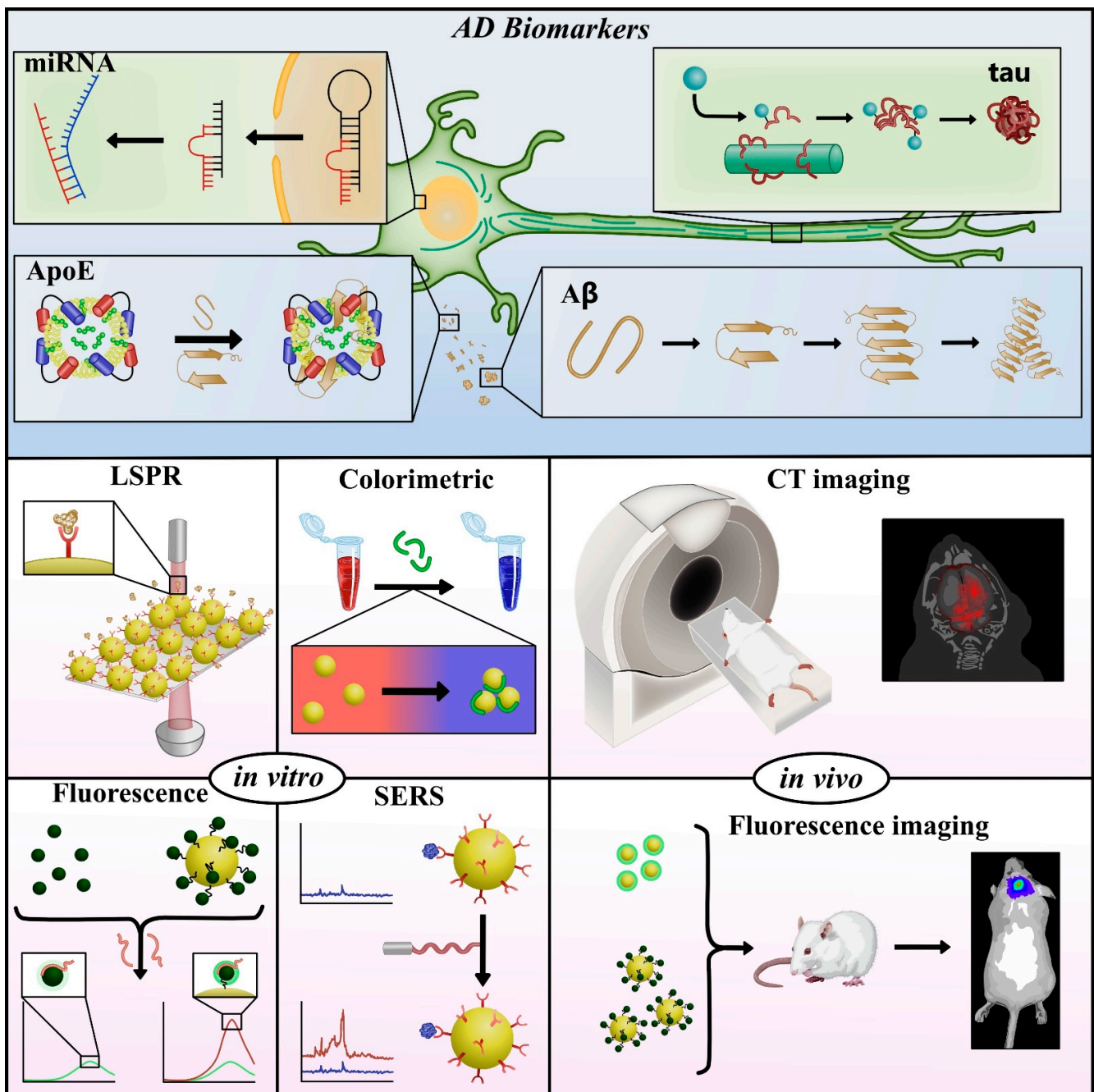


Figure 1. General scheme of optical detection platforms that use plasmonic nanoparticles for detecting *in vitro* Alzheimer's disease (AD) core ($A\beta$ and tau protein) and other biomarkers associated with the development of AD. Due to AD biomarkers are at trace levels in biological fluids such as blood and cerebrospinal fluid (CSF), the development of sensitive and specific methods is highly necessary to detect these biomarkers and establish an early diagnosis and progression of this disease. Considering these aspects, different optical techniques as SERS, fluorescence, colorimetric, and LSPR have been proposed for the detection of AD biomarkers. Additionally, molecular *in vivo* imaging techniques, such as magnetic resonance imaging (MRI) and X-ray computed tomography (CT), have been used to observe structural changes in the brain with AD. Thus, the synergy between the detection of AD biomarkers in biological fluids and imaging techniques could provide an early diagnosis of AD.

2. Relevant AD Biomarkers

Biomarkers constitute physiological, biochemical, and anatomical variables that can be measured *in vitro* and *in vivo* and indicate specific features of disease-related pathological changes [17]. Several biomarkers have been reported to have a specific role in the

development of AD, such as A β peptide in cerebral amyloid deposition and tau protein in neurodegeneration.

In this section, we summarize the characteristics of core AD biomarkers (A β and tau) involved in the formation of senile plaques and NFTs, respectively, as well other AD biomarkers are mentioned, such as ApoE, miRNA, etc.

2.1. Amyloid- β Peptide (A β)

Among the biomarkers that are currently known for AD diagnosis, the most relevant one is the A β peptide, showing a key participation in the development of AD, as described in the amyloid cascade hypothesis [4,18,19] shown in Figure 2A. This hypothesis posits that A β is produced by the processing of the amyloid precursor protein (APP), a transmembrane protein located in the neuronal cell membrane [20,21]. Under physiological conditions, A β is cleared from the brain through the CSF; however, under pathological conditions, A β suffers a state of aggregation through the formation of different intermediate species (Figure 2B), such as dimers, trimers, oligomers (A β Os), protofibrils (A β PFs), and fibers (A β Fs), which eventually are deposited as senile plaques [22,23]. The latter has been observed in the brain of AD patients through imaging techniques used in clinical diagnosis.

AD has been hypothesized to begin 15–20 years (preclinical stage) before the first clinical symptoms are manifested [11]. In the primary stage, A β accumulation and aggregation promote inflammatory processes and aggregation of other proteins, such as the tau protein, increasing neurodegenerative damage [19,24]. At this stage, the patient is cognitively normal and does not reflect any symptom maintaining this condition for decades. Later, A β peptide aggregates into senile plaques at the extracellular level while tau protein aggregates into neurofibrillary tangles at the intracellular level, provoking several symptoms at the brain level that are altogether termed mild cognitive impairment. Thus, both kinds of aggregates start to trigger neuronal death and brain injuries modifying the structure of the brain causing the first symptoms of the disease. When these symptoms get worse, progress to dementia, which is the final stage of AD (Figure 2C).

Therefore, the early detection of these species as clinical biomarkers of AD is very attractive and important to provide timely treatment and limit disease progression.

In particular, the two common isoforms of A β , soluble A β_{1-40} and insoluble A β_{1-42} , are thought to be critical elements in AD pathogenesis. The concentration of soluble A β Os is increased in CSF of AD, compared to control subjects [25] and since this aggregate has been described as highly toxic, it may serve as a biomarker for AD diagnosis [25].

As senile plaques are composed mainly of A β_{1-42} , it has been observed that a decrease in the concentration of free A β_{1-42} in CSF appears to be the earliest detectable biomarker attributed to the development of AD (before clinical symptoms); therefore, its detection could be an interesting strategy for an early diagnosis of this disease. On the other hand, the concentration of A β_{1-40} has been reported to be unaltered in AD; however, the concentration of A β_{1-42} with respect to A β_{1-40} (A $\beta_{1-42}/_{1-40}$ ratio) in CSF is higher than the concentration of A β_{1-42} alone in patients with AD [26]. In recent years, blood analysis has received enormous attention as a non-invasive method for the detection of AD biomarkers, however, it exhibits some limitations, such as the complexity of its matrix, the low amount of proteins from the brain that reach the bloodstream, and the high probability that these proteins become rapidly degraded, metabolized or eliminated from the body [27]. In addition, the majority of these developed methods have failed to validate the clinical utility of quantifying AD biomarkers in blood.

2.2. Tau Protein

Tau is a key protein for microtubule stability in neurons and plays an important role within cell structure and neuronal traffic. Tau protein dysfunction in the brain has been associated with NDDs as AD and other tauopathies. Abnormally, P-tau mainly contributes to forming NFTs inside the brain, which are insoluble aggregates that generate paired helical and straight filaments [8], as shown in Figure 2B.

NFTs, in conjunction with extracellular A β aggregation, have been described as two valuable biomarkers for AD diagnosis [28].

In addition, high concentrations of T-tau and P-tau in CSF—due to cortical neuronal loss and cortical tangle formation, respectively— and low concentrations of A β_{1-42} due to cortical amyloid deposition, have been described as useful biomarkers for AD diagnosis [29,30]. However, due to the CSF extraction is an invasive procedure for patients, the detection of tau levels in blood has also been proposed. More recent research has demonstrated that blood concentration levels of P-tau at threonine 181 (P-tau₁₈₁) could help diagnosis and differentiation of AD from other NDDs [31].

For T-tau and P-tau proteins, the concentration levels in biological fluids that have been reported are very low (195 pg mL⁻¹ or 4.3 pM in CSF [29]). For this reason, the development of highly specific and sensitive analytical techniques is essential. However, currently, the fabrication of new sensing platforms for tau detection has been relatively less than A β peptide detection platforms.

2.3. Other AD Biomarkers

The biomarkers aforementioned are some of the most studied and known for AD due to their participation in the development of this disease; however, a unique biomarker to diagnose AD with high accuracy has not yet been discovered. In this context, the detection of multiple biomarkers has been reported [32,33].

Whereas the function of A β and tau in AD have been described in the literature, the apolipoprotein E4 (ApoE4) is indicated as the most prevalent genetic risk factor in AD. ApoE4 can promote the accumulation of A β in the brain, stimulating its permanence and, subsequently, its aggregation. In fact, high ApoE4 levels in the brain have been associated with a high-risk genetic factor, whereas ApoE2 and ApoE3 have mainly been associated with a protective factor [13,34]. Also, gene mutations have been associated that cause autosomal dominant familial AD are APP on chromosome 21, presenilin-1 (PSEN1) on chromosome 14, and presenilin-2 (PSEN2) on chromosome 1 [35]. On the other hand, some specific miRNAs including miR-9, miR-137, miR-181, and miR-29, associated with immune response and inflammation, have also been related to AD [36].

Due to the large number of novel AD biomarkers that have been reported and reviewed in the literature [32,37,38], in the next sections we will focus on optical detection methods reported using metal nanoparticles for sensing A β , tau, and other biomarkers in clinically relevant fluids.

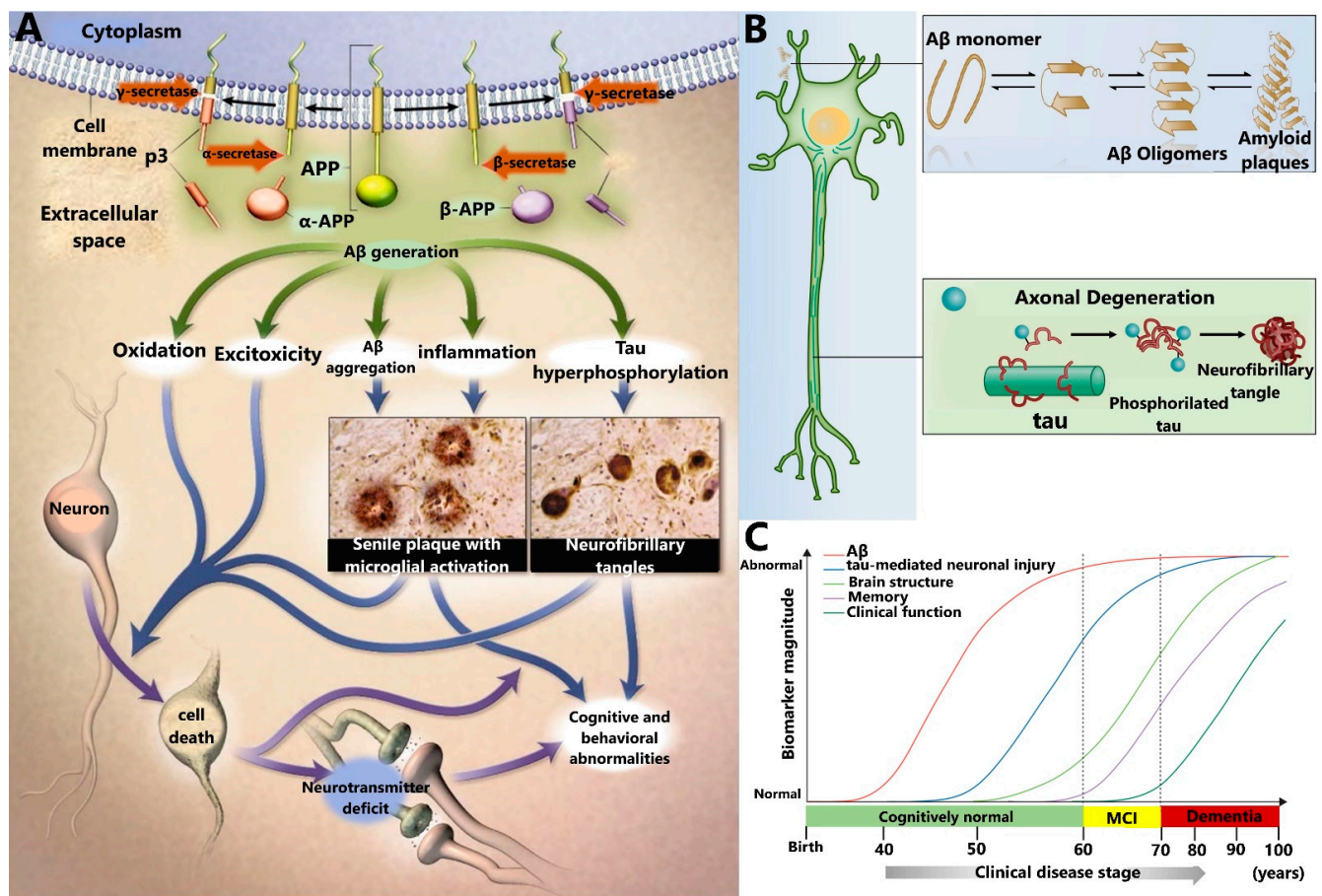


Figure 2. The putative amyloid cascade hypothesis and neuropathological hallmarks of AD. (A) This hypothesis states that AD progresses from the generation of the A β peptide from the amyloid precursor protein (APP), through multiple secondary steps, until reaching cell death. From ref. [39] Copyright © 2021 Massachusetts Medical Society. Reprinted with permission from Massachusetts Medical Society. (B) In the amyloid cascade hypothesis, A β monomers exist in equilibrium with aggregates of higher molecular mass (dimers, trimers, and oligomers), which finally form a deposit of amyloid plaques at the extracellular level. On the other hand, detachment of P-tau from axonal microtubules would destabilize them, resulting in axonal degeneration at the intracellular level and forming the neurofibrillary tangles (NFTs) at the intracellular level. (C) Hypothetical model showing the time-dependent changes in the levels of AD biomarkers. Levels of A β and tau in CSF are identified by PET (positron-emission tomography) and fluorodeoxyglucose-PET. Brain structure is visualized using structural magnetic resonance imaging. MCI: mild cognitive impairment. Republished with permission of Royal Society of Chemistry from ref. [40].

3. Optical Properties of Plasmonic Metal Nanoparticles

The optical properties of metal nanoparticles (NPs) are very important for many of their applications. Noble NPs with a negative real and small positive imaginary dielectric constant, support a localized surface plasmon resonance (LSPR), generated by a collective oscillation of surface conduction electrons that strongly couple with electromagnetic radiation at specific wavelengths (Figure 3, central image) [41–43]. From the interaction of the NPs with incident light, a part of these photons are absorbed and others scattered in different directions [42,44]. Hence, one or more UV-vis extinction bands in the electromagnetic spectrum observed in NPs suspensions include both absorption and scattering components, which are highly enhanced when LSPR is excited [42,45].

The optical cross-sections (absorption and scattering) in spherical NPs has been calculated through Mie's theory that describes the scattering of electromagnetic wave for homogeneous spherical particles solving Maxwell's equations [46]. Furthermore, modify-

ing Mie's theory, it has been possible to include spheroids [47] and for other geometries, a discrete dipole approximation (DDA) has been applied [45].

As a result, the LSPR of NPs is very sensitive to changes in chemical composition, size, shape, or functionalization as well as dielectric permittivity of the environment where they are dispersed [42,43,48]. The chemical composition directly affects the interaction of the NPs with the light, so only noble metals such as Au, Ag, Cu, etc. have an LSPR band in the UV ultraviolet (UV)-visible and near-infrared region (NIR) [49].

The size and shape of NPs are important parameters that allow one to control a wide spectral tunability of LSPR along the UV-vis and NIR of the electromagnetic spectrum [44]. For example, gold nanospheres (AuNSps) with an average size of 16 nm have an absorption band at 520 nm, while 60 nm is located at 535 nm. For silver nanospheres (AgNSps) with a diameter of 5 nm, the LSPR band is at 390 nm and with 60 nm at ~400 nm [42].

For non-spherical NPs, different plasmon modes are observed, being the anisotropic NPs (e.g., rods, plates, prisms, stars) useful for biomedical applications, due to their LSPR is observed in the NIR where the biological transparency window is located [49,50]. For example, in gold nanorods (AuNRs) two resonance peaks are observed, which correspond to a weak transverse band, located in the visible range and a strong longitudinal resonance, located in the NIR region. In irregular-shaped NPs as stars, cubes, and others is common to observe broadened plasmon resonance peaks over a wide range of the electromagnetic spectrum due to a more complicated interaction with the light [49,51]. An example of changing the LSPR in UV-vis-NIR spectra by varying the size and shape are shown in Figure 3A.

Due to the absorption and scattering coefficients of NPs colloids that support LSPR can be several orders of magnitude higher compared to common organic molecules (e.g., $27 \times 10^8 \text{ M}^{-1} \text{ cm}^{-1}$ for 13 nm AuNPs [52]) and displaying intense colors in the visible region, make them suitable for example in colorimetric sensors (Figure 3B) which through the visualization of the color change for the naked-eye of the aggregation of NPs induced by a specific analyte, allows its detection [53]. Consequently, the NPs-based systems can be characterized by optical spectroscopy based on extinction or scattering measurements [44].

The high scattering makes plasmonic NPs suitable for different scattering detection techniques, for example, optical microscopy-based in darkfield and backscattering mode which allows their application in bioimaging. In biosensing, the sensitivity of LSPR to changes in the local refractive index originates from so-called LSPR sensors (Figure 3B).

The amplification of the local electromagnetic field (with increments of even above 10^2 times in some cases [42]), induced by excitation of LSPR in the NPs produces the so-called "hot-spots", which occur in nanoparticle aggregates or regions close to the surface of NPs, such as at sharp edges and tips in single NPs [44]. These hot spots can increase the fluorescence or Raman signals of molecules or substances localized at a certain distance from the surface of the NPs, leading to field enhancement applications as surface-enhanced fluorescence (SEF) and surface-enhanced Raman scattering (SERS), respectively [44,49,53], (Figure 3C).

In addition to their interesting optical properties influenced by composition, size, shape, refractive index, the NPs have other advantages as chemical stability, easy functionalization, large surface area, and the high surface-to-volume ratio [15]; making them useful and versatile materials in nanomedicine area, where usually, for in vitro sensing, gold (AuNPs) and silver (AgNPs) of different sizes and shapes are the most used because they absorb and scatter light in the 350–900 nm spectral range. Moreover, for in vivo studies, AuNPs are the most applied due to their satisfactory biological compatibility [15,48]. Convenient functionalization of plasmonic NPs with a wide variety of functional groups as antibodies, ligands, drugs, DNA, peptides (Figure 3D) [54], has allowed the development of new nanosystems for sensing of biomarkers of different diseases [3,55,56], diagnostic imaging [57,58], targeted drug delivery [59–61] and therapy for the treatment of cancer or neurodegenerative diseases [62].

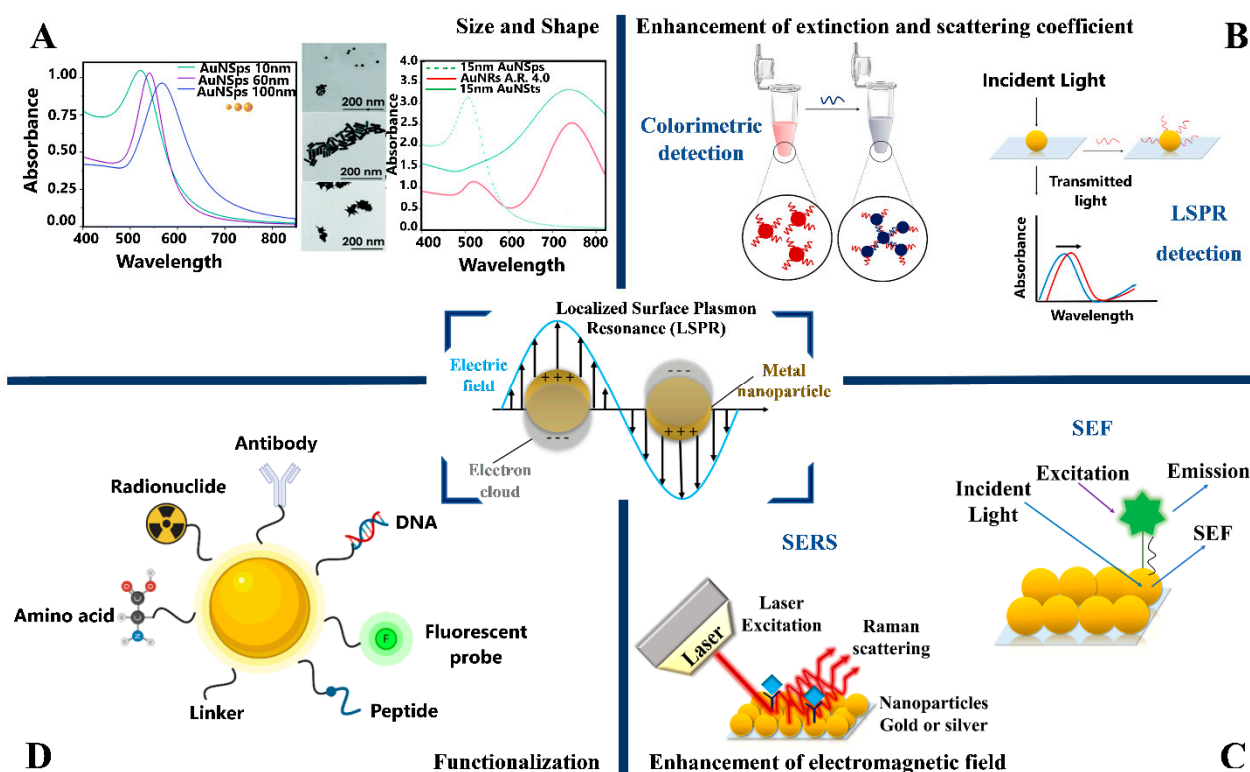


Figure 3. Localized surface plasmon resonance (LSPR) in plasmonic metal nanoparticles. (A) UV-Vis absorption spectra of gold nanospheres (AuNSps) showing the effect of size in LSPR and gold nanoparticles with various geometries: spheres (AuNSps), rods (AuNRs), and stars (AuNSTs). Modified and republished with permission of Royal Society of Chemistry from ref. [63]. (B,C) The LSPR on metal NPs generates different effects, so they can be applied in different optical detection techniques, such as colorimetric, LSPR, SERS, and SEF. (D) The surface of plasmonic NPs can be modified with a wide variety of molecules and biomolecules.

4. Plasmonic Biosensors for In Vitro Optical Detection of AD Biomarkers

Due to the need for an early diagnosis of AD, the development of new platforms for the detection of biomarkers in biological fluids that present sensitivities that apply to the clinic have been continuously sought, within which those based in biosensing technology have become relevant in recent years.

A biosensor is defined as an analytical device composed of a bioreceptor (e.g., antibodies, DNA, cells, fluorescent molecules, etc.), which can recognize a biological target and a transducer that converts a biological response from a biorecognition interaction or reaction into a measurable signal, which can be optical, electrical, magnetic, thermal, etc. [3,8,10]. To provide a sensitive and selective detection, the bioreceptor should exhibit a high affinity or dissociation constant (K_d) towards the specific analyte. It has been reported that bioreceptors with $K_d \sim 10^{-15}$ M can recognize analytes down to fM concentration level [40]. In this context, the most well-established bioreceptors with high dissociation constants are antibodies (10^{-8} – 10^{-12} M) [64] and aptamers (10^{-6} – 10^{-12} M) [40]. Although antibodies are widely used as sensing platforms, some disadvantages have been described such as low stability and higher lot-to-lot variations; on the other hand, aptamers are a promising alternative due to their features as high stability at room temperature, low cost, ease of synthesis, among others [40]. Antibodies and aptamers are the bioreceptors commonly used for sensing AD biomarkers. Other less common alternatives that have emerged recently are fluorescent probes, peptides, and other small molecules, and also label-free platforms.

The incorporation of different types of nanomaterials in biosensors has been considered as a fundamental parameter for enhancing analytical performance characteristics (precision, accuracy, sensitivity, selectivity, etc.). Particularly, plasmonic NPs, have been

integrated into many biosensing platforms mainly due to their optical properties already described in Section 3, since they promote an increase in detection sensitivity, which is observed in the lower limits of detection (LOD) of several orders of magnitude reached [3]. In addition, reliability and robustness are other analytical parameters to be considered for the development and potential clinical application of a sensor [65].

Optical biosensors are the most common sensors containing a bioreceptor element integrated with an optical transducer system. Thus, these optical biosensing platforms measure the interaction between the target analyte and the bioreceptor through changes in Raman signals, absorbance, fluorescence, LSPR, or color changes [40]. For example, the conventional enzyme-linked immunosorbent assay (ELISA) test is a type of optical sensor based on absorption and/or fluorescence, with LODs in the pM range, however, several of the plasmonic biosensors described in the following subsections have achieved sensitivities at fM level.

In the following subsections, we will describe the current advances reported in the development of optical biosensors for different AD biomarkers incorporating mainly plasmonic metal NPs (AuNPs, AgNPs) and hybrid systems, nanowire arrays, nanogap shells structures among others, with in vitro applications such as biological fluids (CSF, blood, etc.) using SERS, SEF, colorimetric sensing and surface plasmon resonance (LSPR) detection.

4.1. Surface-Enhanced Raman Scattering (SERS) Detection

Optical detection techniques based on SERS represent a powerful tool for biosensing applications. The large electromagnetic field generated by the presence of “hot-spots” amplifies the Raman signals of SERS probes binding to a target analyte under the excitation by electromagnetic radiation [66]. While it is generally expected that the strongest SERS enhancement when the frequency of incident photon coincides with the surface plasmon resonance band (LSPR) of the NPs (on-resonance field enhancement), it has also been observed on immobilized nanostructures that the maximum Raman signal intensity occurs if the plasmon band is red-shifted compared to the laser excitation wavelength [67]. Similar results have been observed for AuNRs with different aspect ratios [68], and gold nanotriangles (AuNTs) [69,70], where the correlation between size and SERS enhancement is studied, exhibiting the highest SERS activity under off-resonance conditions, explained by a competition between SERS enhancement and extinction [71].

The nominal performance indicators as LODs and the known enhancements factors (EFs) are commonly used to compare efficiency among different SERS sensing platforms.

For example, for non-aggregated colloidal dispersions, the so-called SERS analytical enhancement factor (AEF) presents reported values between 10^4 – 10^5 . NPs supported on a surface or nanostructured substrates in a dry state, the reported substrate enhancement factor (SEF or EF) are in ranges from 10^5 to 10^6 [65].

For this reason, the use of different plasmonic functional nanostructures as individual nanocrystals (e.g., spherical, triangular, rod or star-shaped) with intrinsic hot spots; hollow/nested or core-shell morphologies with nanoscale interior gaps, branched and film-coupled NPs, disordered assemblies as NPs aggregates; ordered assemblies of NPs as superstructures, supercrystals, clusters, and defined superstructures in 2D and 3D are commonly used in SERS as sensing probes [71].

In this way, great interest has arisen from the development of sensing methods for AD biomarkers, based on SERS nanoprobe as an alternative to fluorescent dyes, which use different strategies in their construction to improve sensitivity and selectivity in the quantitative detection in human fluids, such as serum or CSF [72].

4.1.1. SERS Biosensors for A β Detection

El-Said et al. developed a SERS antibody-antigen assay to determine the concentration of the A β_{1-40} peptide. This A β_{1-40} antibody was immobilized on indium tin oxide (ITO) substrate, modified with AuNPs, and showed the highest intensity in SERS spectra due

to the interactions between the antigen and antibody at the AuNPs array height of 91 nm, with a good correlation between the intensity of the SERS signals and the A β antigen concentration over a range of 100 fg/mL⁻¹ μ g/mL [73].

Another sandwich immunoassay was reported by Yang et al. Silver nanogap shells (AgNGSs) functionalized with A β antibody were synthesized as SERS nanoprobe for the sensitive, selective, and multiplexed detection of A β ₁₋₄₀ and A β ₁₋₄₂ in the blood (Figure 4A). By finely controlling the formation of AgNGSs as plasmonic “hot-spots” on silica nanoparticles (SiNPs) at the one-nanometer resolution, A β ₁₋₄₀ and A β ₁₋₄₂ peptides were detected (Figure 4A) with a LOD of 0.25 pg mL⁻¹ and 0.33 pg mL⁻¹, respectively, which is one order of magnitude lower than the ELISA test. Moreover, the AgNGSs nanoprobe-based assay has a dynamic range for A β detection that is two orders of magnitude higher than ELISA [72].

The detection of small amounts of protein aggregates and the simultaneous knowledge and understanding of conformational changes at low concentrations by a nanofluidics-based SERS detection method was proposed in 2011 by Choi et al. [74]. Based on this study, Choi et al. reported the use of a label-free SERS microfluidics device with 80 nm AuNPs onto a 3-aminopropyltrimethoxysilane (APTMS)-modified glass slide as a SERS active substrate to detect A β ₁₋₄₀ aggregates and investigate the aggregation process, including the formation, consumption of α -helix intermediates and growth to β -sheet structures at a low concentration range of 10 fM to 1 μ M. With these results, the authors indicate that protein aggregation and its resulting conformational characteristics depended on the initial A β concentration, accessing to observe the early stages of the A β aggregation process and better understand the conditions which lead to NDDs, such as AD [75].

Another study that used SERS-based microfluidic devices was recently published by Dallari et al. This device is composed of a low-cost polymeric replica molding (REM) with 3D printing stereolithography processes, where -citrate (cit) and -lipoic acid (LA) capped gold nanospheres (AuNSps) and gold nanostars (AuNSts) were deposited and modified with polydimethylsiloxane (PDMS), leading to the formation of self-assembled monolayers (SAMs). This AuNPs-PDMS device was coupled with a portable Raman fiber probe and tested in an aqueous solution of Rhodamine 6G (Rh6G) and 4 μ M of A β ₁₋₄₂ peptide. Consistent with Rh6G results, the A β Raman spectra showed that the intensity of characteristic peaks was higher in the presence of metallic nanostructures (with which the plasmonic band is in resonance with the excitation wavelength), while for bare PDMS, the Raman profile was almost not visible. A 2 to 5-fold increase in the intensity of some A β Raman signals was observed for cit-AuNSts and LA-AuNSts, respectively, due to the presence of “hot-spots” [76].

On the other hand, the concept of SERS-on-fiber technology for diagnostic purposes has been recently developed by the same research group [63]. The integration of a cap SERS-active substrate composed of AuNSps, AuNSts, and CTAB-capped gold nanorods (AuNRs) is assembled in PDMS on the tip of an optical fiber, as shown in Figure 4B. Of the three types of NPs used, AuNSts modified-PDMS caps obtained the highest values of AEF due to the shape of these nanostructures increases the possibility of “hot spots” formation. Functionalization of the NPs with a specific antibody for the A β ₁₋₄₂ monomer (anti-A β) allowed SERS detection of A β at the μ M level, obtaining an increase of 100-fold in Raman signals in the NPs-decorated caps, with similar behavior for AuNRs and AuNSts, respectively [63]. These results show that metal nanostructures are useful for the detection of target analytes and generate a SERS-enhancement effect.

Compared to the conventional SERS substrates, the use of three-dimensional (3D) nanostructures has been explored to increase the density of metal nanostructures that support LSPR [77]. Nanowire arrays (NWs), acting as frameworks, show a Raman signal sensitivity significantly higher than that of a planar framework of AuNPs two-dimensionally adsorbed on a flat surface [77]. Lin et al. fabricated ordered hexagonal-packed silicon nanorod arrays (SiNRs) functionalized with AuNPs (SiNRs@AuNPs) as SERS substrates for the ultrasensitive detection of A β aggregates. By tuning the gap, diameter, and length

of the SiNRs, the substrate exhibits stable and reproducible Raman signals, allowing its application in the detection of long A β fibrils at a single fibril level, which reveals the secondary structure of A β fibrils with high sensitivity and provides a potential method for the study of the dynamic interaction of label-free amyloid protein [77].

Recently, Xia et al. have developed bifunctional NPs for detecting and imaging purposes. AuNPs were functionalized with Rose Bengal dye (RB-AuNPs) and allowed the SERS-based in vitro detection of A β_{1-42} between 0–2 μ M, showing high selectivity due to the affinity between RB and A β [78]. In addition, confocal imaging of amyloid plaques in brain slices from transgenic mice revealed an age-dependent amyloid deposition [78], consistent with previous studies [79].

4.1.2. SERS Biosensors for Tau Detection

Zengin et al. developed a system based on silica-coated magnetic NPs (γ -Fe $_2$ O $_3$ @SiO $_2$) functionalized with monoclonal anti-tau antibody and sandwiched with AuNPs modified with polyclonal anti-tau and 5,5-dithiobis (2-dinitrobenzoic acid) -DTNB- for the ultrasensitive detection of tau protein. Thus, the SERS intensity peak at 1332 cm $^{-1}$ of DTNB allowed the detection of tau with a LOD lower than 25 fM [80].

In comparison to Zengin et al., Maurer et al. reported a sandwich assay to detect tau in CSF, simplifying the magnetic component by Fe $_x$ O $_y$ NPs functionalized with polyclonal anti-tau antibody (Figure 4C). This approach reduced synthesis time and the workload for preparing the whole tau protein-specific immunosensor and can be transferred to other protein biomarkers, by exchanging the specific antibody [81].

4.1.3. SERS Biosensors for the Simultaneous Detection of A β and Tau

Sinha et al. designed magnetic core-plasmonic gold shell NPs decorated hybrid 3D graphene oxide (GO) as a robust 3D SERS platform with a high number of “hot-spots” for the detection of A β and tau in whole blood samples. The AEF value for the 3D SERS substrate was about 5 orders of magnitude higher than that of plasmonic NPs (0D) alone and more than 9 orders of magnitude higher than 2D GO, and allowed the high capture and fingerprint identification of trace levels of A β and tau protein, with a LOD of 500 fg/mL and 0.15 ng/mL, respectively [82], values which are several orders of magnitude higher than the currently used technology in clinics.

Another highly sensitive and selective SERS-platform was reported by Demeritte et al. Iron-gold core-shell NPs attached to hybrid graphene oxide (HGO) allowed the selective separation and accurate identification of A β and tau from whole blood samples. The results revealed that the multifunctional HGO nanoplatform can be used as a SERS “fingerprint” for A β and tau detection in concentrations as low as 100 fg/mL, with a LOD several orders of magnitude higher than that of the ELISA kit for A β (0.312 ng/mL) and tau protein (0.15 ng/mL) [83]. The high sensitivity obtained is attributed to strong plasmon-coupling, which generates huge amplified electromagnetic fields at the “hot spots”. Furthermore, the nanoplatform can distinguish A β and tau biomarkers from human serum albumin (HSA), which is one of the most abundant proteins in the CSF.

Recently, Park et al. created a carboxylic-acid-functionalized and graphitic nanolayer-coated label-free 3D-SERS sensing platform (Figure 4D) composed of well-defined and uniform gold nanowire arrays (AuNWs). An AEF of 5.5×10^5 , comparable with reported AEF values for similar 3D SERS substrates [84,85], allowed the detection of conformational changes and the concentration of A β and tau proteins, with linear ranges of 10^{-7} M to 10^{-9} M and 10^{-8} M to 10^{-11} M, respectively [86].

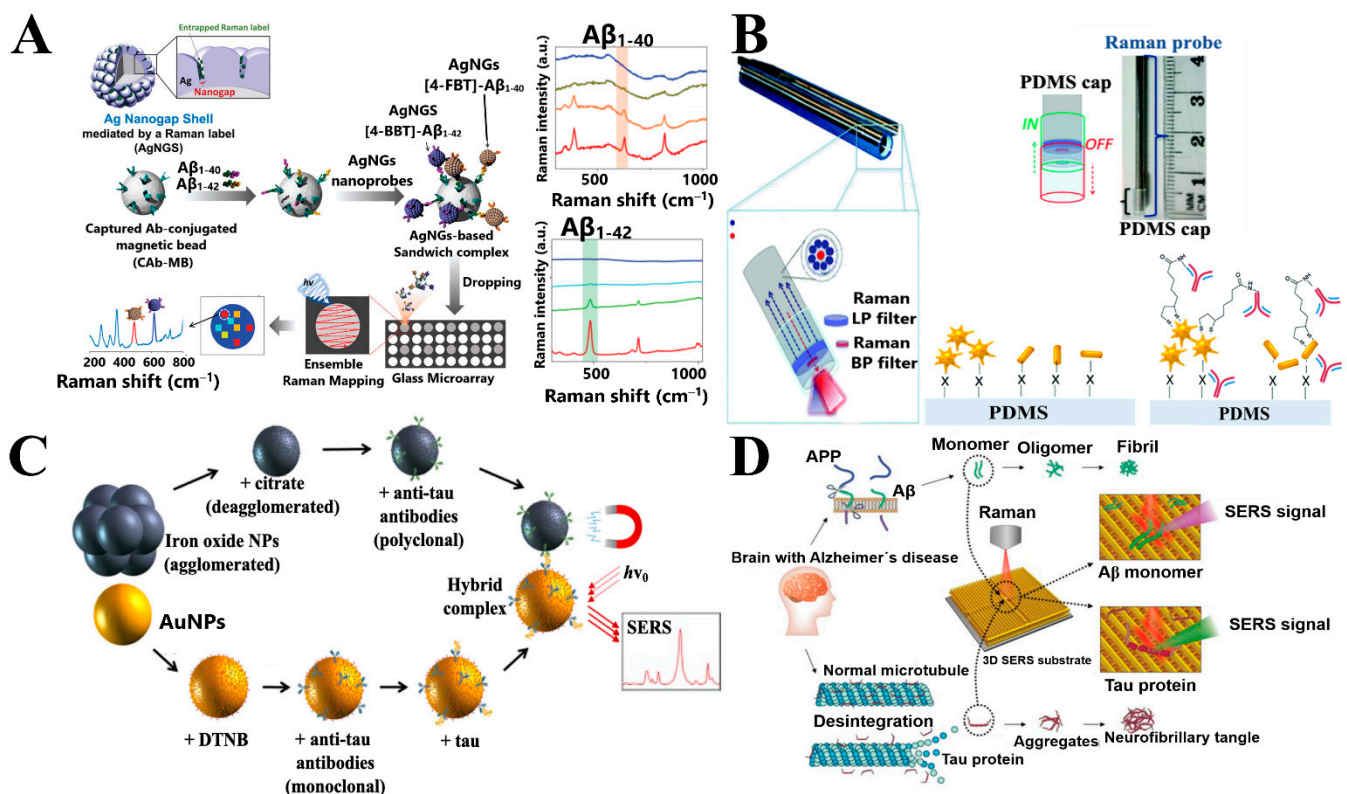


Figure 4. SERS nanoplasmonic platforms for AD biomarkers. (A) Schematic illustration for the multiplexed detection of $A\beta_{1-40}$ and $A\beta_{1-42}$, using $A\beta$ antibody-conjugated AgNGS nanoprobes in a sandwich immunoassay. Representative Raman spectra for $A\beta_{1-40}$ and $A\beta_{1-42}$ were obtained with the proposed system. Reproduced with permission of Wiley Materials from ref. [72]. (B) Graphic description of NPs-modified PDMS caps which can be inserted or removed from the distal end of the Raman probe using AuNSts and AuNRs on PDMS substrates. Republished with permission of Royal Society of Chemistry from ref. [63]. (C) Schematic depiction illustrating the formation of the hybrid complex with the individual experimental steps. Reproduced with permission of Wiley Materials from ref. [81] (D) Graphical scheme of 3D SERS-substrate for sensitive $A\beta$ and tau detection. Adapted with permission from ref. [86]. Copyright 2020 American Chemical Society.

Hybrid bionanomaterials, such as DNA-AuNPs conjugates, provide excellent platforms for chemical and biological applications. In particular, the use of poly adenine (polyA) can serve as an anchoring block for preferential binding with AuNPs surfaces [87], and the appended recognition block can form an upright conformation that benefits DNA hybridization. These nanomaterials have been applied for the detection of DNA and small molecules, but not proteins. However, Zhang et al. developed a robust and sensible SERS biosensing platform for the detection of $A\beta$ Os ($A\beta_{1-42}$) and tau. Using different Raman dye-coded (polyA) aptamer-gold nanoparticles (PAapt-AuNPs) conjugates, the specific protein-aptamer binding induced the aggregation of AuNPs and the plasmonic coupling effect of “turning on” SERS detection of target biomarkers. This strategy displayed excellent analytical performance for the detection of $A\beta$ Os and tau, with a LOD of 3.7×10^{-2} nM and 4.2×10^{-4} pM, respectively. In addition, $A\beta$ Os and tau were detected in artificial CSF (aCSF), with high recovery percentages (96–98% and 97–99%, respectively) [88].

4.1.4. SERS Biosensors for Other Biomarkers

A recent clinical study in AD patients was reported by Carlomagno et al., who developed an innovative SERS-based biosensor using 35 nm AgNPs to analyze human serum from AD patients well-characterized from an A/T/N (A = amyloid, T = tau; N = neurodegeneration) perspective, versus healthy subjects. After optimizing different parameters, the SERS results demonstrated a statistical difference between the spectra collected from the

two experimental groups, with accuracy, precision, and specificity of 83%, 86%, and 86%, respectively. On the other hand, the authors found a direct relationship between brain tissue degeneration visualized by magnetic resonance imaging (MRI) and the appearance of a specific biochemical pattern from SERS data in serum collected from AD patients, showing that SERS is a potential label-free tool for monitoring AD progression and rehabilitation treatments in a minimally invasive way [89].

4.2. Fluorescence-Based Sensing Platforms

Fluorescence-based biosensors have also been developed for the detection of different biologic analytes. Using plasmonic NPs, the LSPR can generate two effects on the emission of a fluorophore, depending on the fluorophore-nanoparticle distance: fluorescence quenching or enhanced fluorescence intensity [52]. Thus, if the distance is less than 5 nm, fluorescence quenching occurs, due to the energy of the excited fluorophore is totally transferred to NP [52]. For distances from 5 nm or more, an increase in the fluorescence of a quantum emitter has been reported. This enhancement effect in fluorescence due to the presence of metal NPs has been attributed mainly to two factors: (i) increase in the excitation efficiency of the molecules placed near to local electric fields of the NPs and (ii) increase in the radiative decay rate of the fluorophore due to re-radiation by the plasmonic NPs [52].

4.2.1. Fluorescent Biosensors for A β Detection

Xia et al. reported a label-free fluorescent detection method for A β Os based on the quenching efficiency of AuNPs through the inner filter effect (IFE) on the fluorescence of cadmium telluride quantum dots (CdTe-QDs), as illustrated in Figure 5A. This method enabled the quantification of A β Os with a LOD of 0.2 nM, with high selectivity, due to the specific recognition of A β Os by PrP (95–110) [90].

Saini and Sadhu reported that AuNPs quenched the fluorescence of the SEA-SC2 probe, which was recovered after treatment with A β monomers, showing a stronger affinity between A β monomers and AuNPs, compared to their affinity towards SEA-SC2. Furthermore, in the presence of Cu²⁺ ions, the formation of the A β -Cu²⁺ complex resulted in a greater rapid fluorescence enhancement using SEA-SC2 (Figure 5B). Thus, this method allowed the detection of A β _{1–40} and A β _{1–42} monomers at pH 7.4 in a concentration range of 10–60 nM. In addition, the methodology was used to evaluate aCSF and HSA samples and revealed that the detection of A β _{1–40} monomers was 1.5 times more efficient than for A β _{1–42} at 60 nM in aCSF [91].

DNA molecular machines, in particular, DNA walkers, are considered attractive amplification strategies due to the advantage of the signal enhancement cascade generated by its autonomous movement [92]. Yin et al. designed a 3D DNA walker nanoprobe for the sensitive detection and real-time in situ imaging of A β Os. The DNA walker nanoprobe composed of AuNPs modified with aptamer-Zn²⁺-dependent DNAzyme walking strands and TAMRA-labeled hairpin substrate strands (Figure 5C) enabled the in vitro fluorescence detection of A β Os in the concentration range of 0.1–1.0 nM, with a LOD of 22.3 pM, as shown in Figure 5C [92].

Based on the enhancement fluorescence effect, Jara-Guajardo et al. reported that AuNRs functionalized with D1 peptide (AuNRs-PEG-D1), and through the measurement of the fluorescence intensity of the near-infrared (NIR) fluorescent probe CRANAD-2, improved the in vitro detection of A β _{1–42} aggregates. AuNRs-PEG-D1 at concentrations of 0.1 nM and 0.5 nM increased the fluorescence of CRANAD-2 bound to A β fibrils (2 and 3-fold, respectively), allowing its detection at μ M concentrations. Furthermore, the methodology was validated ex-vivo in brain slices of transgenic mice and allowed the detection of amyloid plaques, which accounts for the potential applicability of this detection technique to living organisms [93].

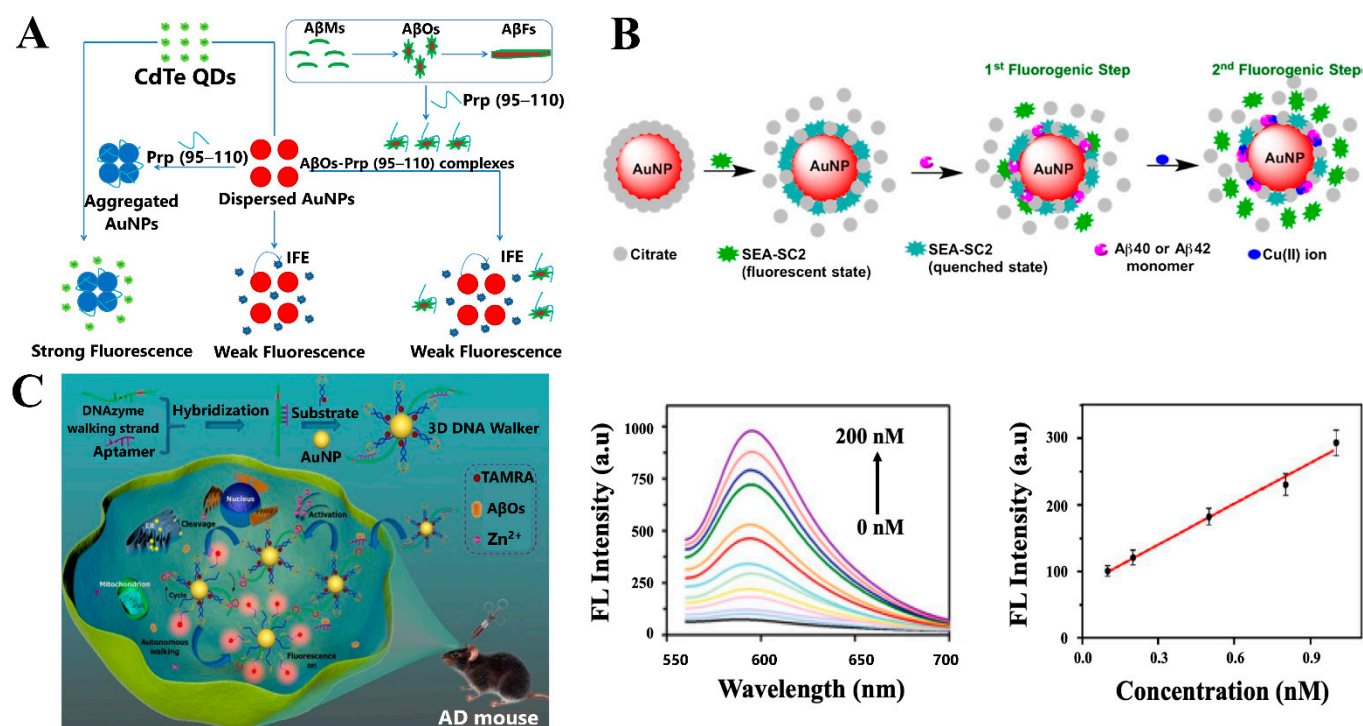


Figure 5. Examples of fluorescent sensors using NPs. (A) Schematic illustration of the visual and fluorescent detection of AβOs through the inner filter effect (IFE) of AuNPs on the fluorescence of CdTe-QDs. In the presence of AuNPs, the emission of CdTe-QDs is significantly quenched. The AβOs-PrP (95–110) complex can be adsorbed onto the surface of the AuNPs, thus triggering the aggregation and color change of the AuNPs suspension. As a result, the IFE of AuNPs on the fluorescence of CdTe-QDs is weakened and fluorescence intensity is recovered. Upon addition of Aβ samples to the PrP (95–110) solution, PrP (95–110) interacted specifically with AβOs, thus losing the capability to induce AuNPs aggregation. Reprinted from ref. [90], Copyright 2016, with permission from Elsevier. (B) Strategy for the detection of the Aβ monomer in the presence of AuNPs and the small fluorophore SEA-SC2. Reprinted from ref. [91], Copyright 2020, with permission from Elsevier. (C) Schematic illustration of AβOs sensitive assay, based on the target-triggered DNAzyme-driven 3D DNA walker fluorescence signal amplification technology; fluorescence spectra of the 3D DNA walker nanoprobe in the presence of different concentrations of AβOs (0~200 nM) and linear plot of fluorescence intensity versus the corresponding AβOs concentrations. Reprinted with permission from ref. [92]. Copyright 2020 American Chemical Society.

4.2.2. Fluorescent Biosensors for Other AD Biomarkers

Han et al. developed a chemical tongue sensor array using 4 kinds of fluorescent gold nanoclusters (AuNCs), with different surface properties for protein discrimination in the nM range. A linear discrimination analysis (LDA) based on fluorescence intensity response patterns was used and 8 proteins with diverse isoelectric points and molecular weights were effectively discriminated in the urine. In addition, the specific protein types detected in serum samples from AD patients could be discriminated from those of osteoarthritis patients and healthy people [94].

4.3. Colorimetric Detection

Colorimetric sensors are widely used for the detection and quantification of different analytes. Because the colorimetric response can be followed by visualizing the color change of a solution with the naked eye, this technique is very attractive due to its simplicity (without the use of sophisticated instruments), speed, and low-cost compared with other detection methods [95]. Particularly, the use of plasmonic NPs, such as AuNPs and AgNPs, is widespread in colorimetric assays due to the characteristic color change following mode shift (aggregation and non-aggregation) in the presence of a target analyte, which would allow its application for the detection of different AD biomarkers.

4.3.1. Colorimetric Biosensors for A β Detection

Ferriprotoporphyrin IX (Heme) has been associated with AD because it can bind through 3 histidine residues to A β forming a heme-A β complex, which causes a stabilization of the A β peptide structure and therefore inhibits its aggregation process. Moreover, Cu²⁺ can be linked to A β through 2 histidine residues, thus forming a Cu-A β complex. Yu et al. developed a rapid and sensitive colorimetric method to determine total monomeric A β in a rat model of AD. Polyethyleneimine gold nanoparticles (PEI-AuNPs) modified with Cu²⁺ and hemin (PEI/AuNPs-Cu-hemin) allowed the detection of A β species through double molecular recognitions, forming a Cu-A β -hemin complex and resulting in the aggregation of the NPs with a color change from red to blue (Figure 6A). This method displayed high sensitivity towards total A β monomers (A β ₁₋₁₆, A β ₁₋₄₀ and A β ₁₋₄₂) (Figure 6A) within a linear range from 0.2–5000 ng mL⁻¹ and presented a LOD ~ 40 pg mL⁻¹ [96]. Zhou et al. reported a simpler colorimetric sensing system for A β ₁₋₄₀ detection in aqueous media based on the aggregation of AuNPs in the presence of Cu²⁺ [97]. The AuNPs conjugated with A β ₁₋₄₀ and coordinated with Cu²⁺ generated a color change from red to blue, according to the aggregation of the AuNPs, and allowed the detection of A β ₁₋₄₀ with a LOD of 0.6 nM and application in human serum with acceptable accuracy.

Ghasemi et al. established a label-free colorimetric detection of A β ₁₋₄₀ and A β ₁₋₄₂. Conjugated AuNPs and AgNPs with A β ₁₋₄₀ and A β ₁₋₄₂ peptides and coordinated with Cu²⁺, produced the aggregation of NPs and therefore different color changes. With this method, was possible the detection and discrimination of both A β ₁₋₄₀ and A β ₁₋₄₂ from human serum albumin (HSA) between 50 nmol L⁻¹–500 nmol L⁻¹ concentration levels. Also, this colorimetric sensor allowed the detection of similar A β peptides in plasma samples [98].

On the other hand, Hu et al. developed a colorimetric sandwich immunosensor based on AuNPs coated with -N and -C terminal A β ₁₋₄₂ antibodies (AuNPs@C/N-Ab₁₋₄₂), which can detect A β ₁₋₄₂ owing to the specific binding of N- and C-terminal antibodies, generating the aggregation of AuNPs@C/N-Ab₁₋₄₂, which produce a color change from red to blue (Figure 6B). With a linear range from 7.5–350 nM and LOD of 2.3 nM, which is equal or better than other reported methods, this immunosensor allows simple and specific detection of A β ₁₋₄₂. Furthermore, it can be applied in real blood samples, with high recovery percentages [99]. The same research group also developed a similar immunosensor with AgNPs. This study used a C-terminal A β _{1-40/1-42} antibody conjugated with AgNPs (Ab-AgNPs) for the specific and selective detection of A β _{1-40/1-42}. The binding between A β _{1-40/1-42} peptides and Cu²⁺ produces the aggregation of Ab-AgNPs, and a color change from yellow to red (Figure 6C). This immune-sensing approach detected A β _{1-40/1-42} in the 0.25–150 nM concentration range, with a LOD of 86 pM, which is equal or better than LODs reported for other assays (ELISA and others). Finally, the immunosensor was applied to real blood samples, with high recovery percentages (~99%) [100].

On the other hand, Zhu et al. developed a colorimetric aptasensor based on cit-AuNPs for the detection of A β Os (A β ₁₋₄₀), by monitoring the UV-Vis spectrum in the aggregation/stabilization of the AuNPs-aptamer in the presence of A β Os (Figure 6D). This aptasensor presented a linear range of 1–600 nM and a LOD of 0.56 nM, and detected A β Os in aCSF samples, with recovery percentages between 92–101% [101].

Li et al. used polyoxometalate (POM)/A β ₁₅₋₂₀ coated-AuNRs for the colorimetric detection of A β ₁₋₄₀ aggregates. The A β ₁₋₄₀ aggregation process can be visualized by the naked eye by observing the color change from brown to blue produced when the A β aggregates induce AuNRs precipitation; this produces a shift in the LSPR that intensifies as the concentration of A β ₁₋₄₀ aggregates increases [102]. Moreover, the proposed system was applied as a chemotherapeutic agent and for the photothermal treatment of AD.

4.3.2. Colorimetric Biosensors for the Detection of Other AD Biomarkers

Colorimetric methods have also been proposed for the detection of other AD biomarkers.

miR-137 has demonstrated its potential as a non-invasive biomarker in blood for AD diagnosis and prognosis [36]. Delkhahi et al. reported a new sensitive and specific microRNA assay based on colorimetric detection of AuNPs using DNA hybridization chain reaction amplification (HCR). This method can detect miR-137 with a LOD of 0.25 nM [36], allowing its application in real blood samples without the need for sample preparation, RNA extraction, and/or amplification.

Altered concentrations of proteins such as Fetuins and Clusterin have been related to AD [33]. Considering these antecedents, Brazaca et al. developed a microfluidic paper-based analytical device (μ PAD) with colorimetric detection, using selective antibodies immobilized on AuNPs for the simultaneous quantification of Fetuin B and Clusterin (Figure 6E). Through the analysis of color intensity, Fetuin B and Clusterin were detected in the range of 0.1–500 nM and 0.1–1000 nM, with a LOD of 0.24 and 0.12 nM, respectively [33], making this biosensor a great potential for the early detection of AD.

Ren et al. reported a sandwich-type colorimetric immunosensor for the detection of ApoE, using specific anti-ApoE “nanobodies” as the capture and detection antibodies on ITO-AuNPs surface and a gold-TiO₂-glucose oxidase (GOx) support. Through the catalysis of glucose to H₂O₂ by GOx, ApoE was detected with a LOD of 0.42 pg/mL, and the clinical analysis achieved a satisfactory performance [103].

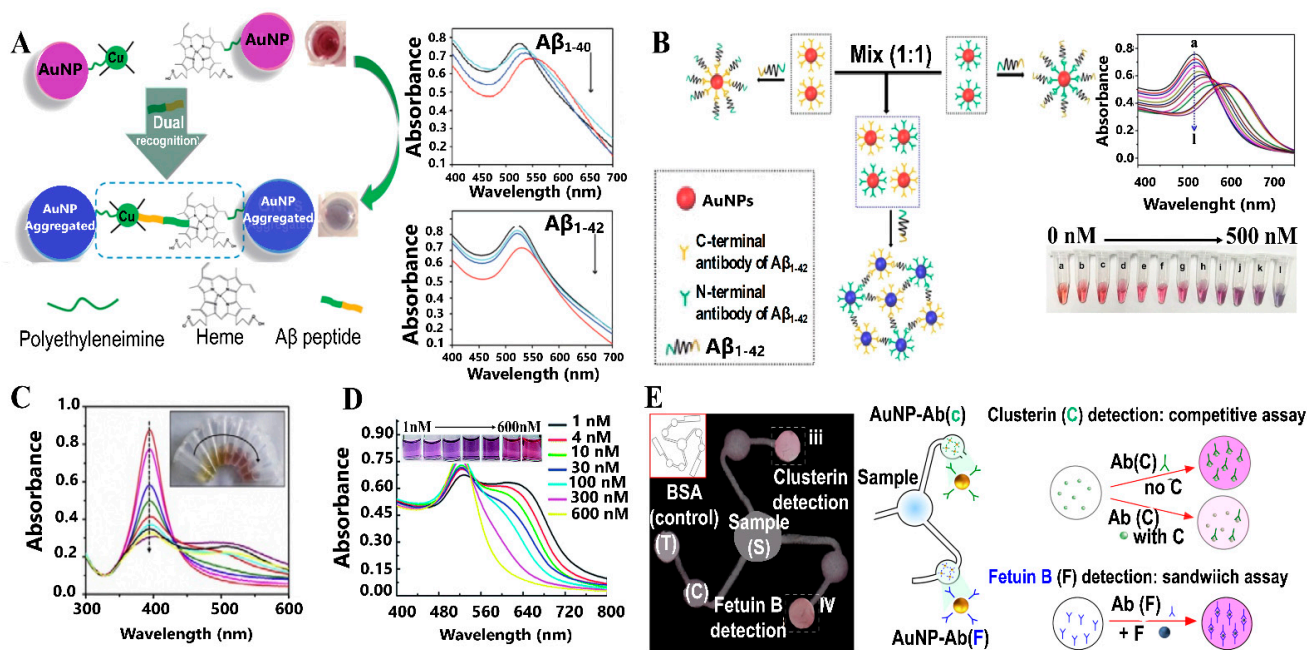


Figure 6. Different colorimetric sensing platforms using NPs. (A) Colorimetric sensing of A β based on the PEI/AuNPs-Cu-hemin probe; UV-Vis spectra of the PEI/AuNPs-Cu-hemin probe before (in black) and after incubation with different concentrations of A β ₁₋₄₀ and A β ₁₋₄₂. Republished with permission of Royal Society of Chemistry, from ref. [96]. (B) The principle of the AuNPs@C/N-Ab₁₋₄₂ colorimetric sandwich immunosensor for A β ₁₋₄₂; absorption profile of the AuNPs@C/N-Ab₁₋₄₂ colorimetric sandwich immunosensor system with increasing concentrations of A β ₁₋₄₂, from 0 to 500 nM. Reprinted from ref. [99], Copyright 2017, with permission from Elsevier. (C) Absorption profile of the Cu²⁺-Ab-AgNPs colorimetric immunosensor with increasing concentrations of A β _{1-40/1-42}, from 0 to 300 nM. Reprinted from ref. [100], Copyright 2016, with permission from Elsevier. (D) Absorption spectra of the AuNPs-based colorimetric assay in the presence of various concentrations of A β Os. Republished with permission of Royal Society of Chemistry, from ref. [101]. (E) Lateral flow paper device for the detection of clusterin and fetuin B, including sample (S), conjugation (C), and test (T) areas. The selective antibodies for clusterin (C) and fetuin B (F) are immobilized on AuNPs and loaded on the conjugation zone. The strategy used to detect clusterin was based on a competitive assay in which clusterin immobilized on the test zone competes for the AuNPs-Ab with the protein present in the sample. For fetuin B, a sandwich strategy is used, relying on antibody immobilization on the test zone and a combination of analyte and AuNPs-Ab on this zone. Reprinted with permission from ref. [33]. Copyright 2019 American Chemical Society.

4.4. Localized Surface Plasmon Resonance Detection Platforms

LSPR is a particular type of SPR technique. The localized plasmons in metal NPs are formed by coupling with photons at certain wavelengths. Thus, the signal transduction mechanism of LSPR platforms is based on their sensitivity to local refractive index changes (as a shift of extinction wavelength) near the surface of -size and -shape-controlled AuNPs and AgNPs after specific recognition between a biomarker and a recognition element [40,104]. So far, some studies have reported the use of LSPR for the detection of AD in fluids.

4.4.1. LSPR Biosensors for A β Detection

Kang et al. developed an AuNPs-LSPR sensor for A β_{1-42} by inducing its aggregation with ApoE4. The AuNPs acted as a catalytic activator and optical reporter, while ApoE4 acted as a chaperon to monitor A β_{1-42} aggregation, with significant changes in the UV-Vis spectra in the presence of ApoE4 (blue curve, Figure 7A). Under physiological conditions (CSF), the LOD was 1.5 pM [105], demonstrating that ApoE4 induces A β_{1-42} aggregation with high specificity, compared to A β_{1-40} (Figure 7A).

4.4.2. LSPR Biosensors for Tau Detection

Recently, Kim et al. proposed an aspect-ratio-3.67 AuNRs-mAb as an LSPR biosensor to detect tau in human plasma. To enhance detection sensitivity, guanidine hydrochloride (Gua-HCl) was used as a chaotropic agent, which interrupts water molecules networks and weakens the hydrophobic interactions between proteins. This allowed the ultrasensitive detection of tau in plasma in the fM range, with a LOD of approximately 100 fM [106]. In addition, this system can accurately diagnose AD in blood samples from AD patients due to the higher LSPR shifts produced with the chaotropic agent, compared to the shifts produced in its absence (gray and black bars in Figure 7B, respectively).

4.4.3. LSPR Biosensors for the Simultaneous Detection of A β and Tau

A multiplexed LSPR immunosensor for A β_{1-40} , A β_{1-42} , and tau using 50 nm AuNSps, and AuNRs with aspect ratios of 1.6 and 3.6, modified with their respective antibodies was developed by Kim, et al. (Figure 7C). Depending on the shape of the NPs (sphere or rod) and the aspect ratio of the AuNRs, the determination of each biomarker was achieved under physiological conditions of mimicked plasma. Thus, each NP interacted with their corresponding biomarker and generated a significant LSPR peak shift (Figure 7C), allowing detection of A β_{1-40} with AuNSps, A β_{1-42} with AuNRs of aspect ratio 1.6, and tau with AuNRs of aspect ratio 3.6, with LODs of 34.9 fM, 26 fM, and 23.6 fM, respectively [107].

Recent evidence has indicated that the levels of the complex formed between tau and A β (tau-A β) could be related to AD progression [108]. Springer et al. developed a new LSPR biosensor for the tau-A β complex, based on a sandwich assay that incorporates thiol functionalized AuNPs (S-AuNPs) (Figure 7D). The interaction or binding of the target analyte with the sensor surface, resulted in a change of the refractive index and therefore a shift in wavelength, which allowed the detection of the tau-A β complex in 10% of CSF and with a LOD of ~0.1 pM (Figure 7D). On the other hand, a LOD of ~1 pM was obtained from real CSF samples from healthy patients. Although this value is low, it would not allow the detection of the tau-A β complex in people with AD whose levels of this biomarker are lower [108]. These preliminary results are a beginning to establish new methodologies to improve the LOD of this AD biomarker.

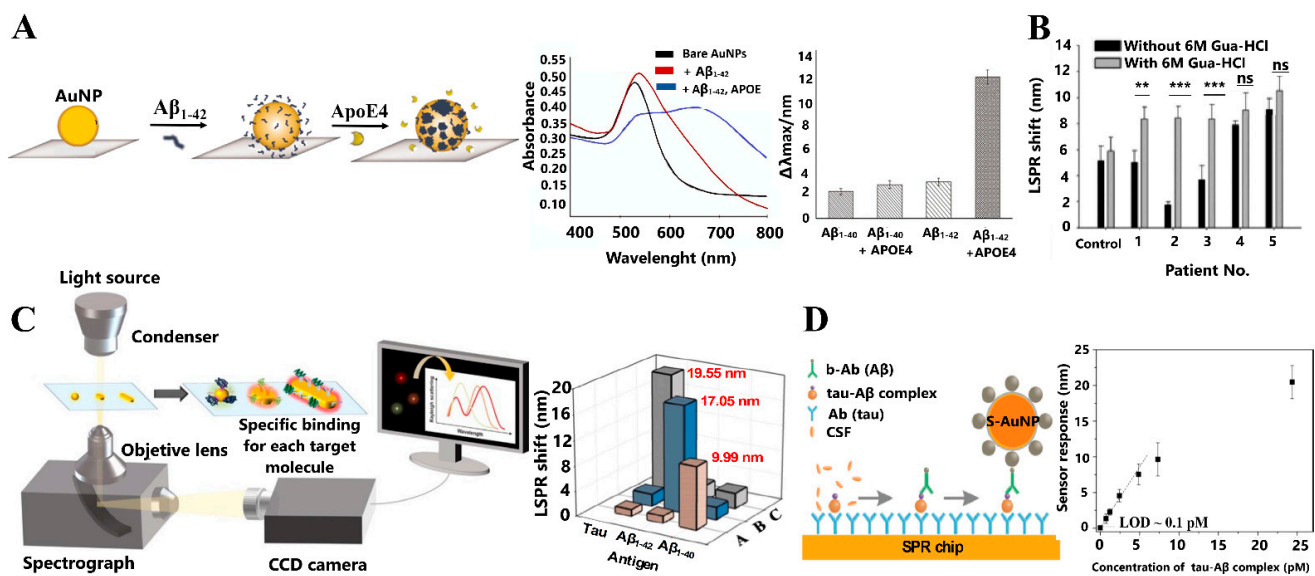


Figure 7. Different sensors for LSPR detection of AD biomarkers. (A) APOE4-mediated β -amyloid aggregation sensor. UV-vis absorption spectra of AuNPs after exposure to A β and ApoE4 with their respective LSPR λ_{\max} shifts (nm). Reprinted from ref. [105], Copyright 2015, with permission from Elsevier. (B) LSPR shifts (nm) of the nanoplasmonic sensor to detect tau in blood samples from controls and AD patients (patients no. 1–5), combined with 6 M Gua-HCl. Data are means \pm SD from three independent experiments ($n = 20$ single AuNRs examined for each experiment). ** $p < 0.001$, *** $p < 0.0001$ (Student's t -test). Reprinted with permission from ref. [106]. Copyright 2019 American Chemical Society. (C) Schematic illustration of a shape-code plasmonic biosensor with their LSPR peak shift (nm) for the independent detection of A β_{1-40} , A β_{1-42} , and tau. Reprinted from ref. [107], Copyright 2018, with permission from Elsevier. (D) Scheme of the assay for the detection of the tau-A β complex and calibration curve for the S-GNP-enhanced detection of the tau-A β complex in 10% CSF. The sensor response is expressed in terms of a shift (nm) in the wavelength at which the SPR dip occurs and is proportional to a change in the refractive index caused by the binding of molecules to the sensor's surface. Reprinted from ref. [108], Copyright 2020, with permission from Elsevier.

4.4.4. LSPR Biosensors for Kinetic Studies of A β Aggregation

Changes in LSPR can also be applied to kinetic studies of biomolecular interactions. NDDs such as AD exhibit a common characteristic mechanism that involves an aggregation process due to protein misfolding [109,110]. This aggregation process promotes the generation of different kinds of species, starting from monomers that assemble into dimers, tetramers, oligomers, and finally, fibrils [111,112]; the latter corresponds to the stable form of the aggregation process and possesses a highly organized structure of cross- β sheets. The intermediate species have been described as the most toxic ones, which provoke neuronal death [113–115]. In fact, the generation of these different aggregation species dictates the onset and progression of the disease.

Commonly, the kinetics of protein aggregation is often inferred from a thioflavin T (ThT) or a Congo red fluorescence assay, which report the following three stages of the pathway that leads to the amyloid state: protein nucleation, elongation, and saturation [116–118]. However, these fibril-specific dyes have sensitivities in the μ M range [119,120] and are not sensitive to the early formed oligomers, limiting their use in detecting oligomeric species [121].

Due to the high sensitivity of LSPR of metal NPs towards changes in the local refractive index and dielectric properties [121], the use of LSPR as a detection tool for AD would allow the sensitive measurement of NPs-protein interactions and detection of the species formed in the aggregation process in real-time and in a label-free mode.

Elbassal et al. performed a study with sub-micromolar sensitivity to monitor the A β_{1-40} aggregation kinetics of A β Fs and A β Os using the changes produced in the LSPR band of AuNSps. For A β Fs formation, after 24 h incubation of monomers, the intensity

of the LSPR band of AuNPs gradually increased, compared with AuNPs- $A\beta_{1-40}$ ($A\beta$ concentration-dependent) and increased with time, according to the fibrillization kinetics of $A\beta_{1-40}$ (Figure 8A). Furthermore, the LSPR band intensity was sensitive to the presence of $A\beta$ O for both $A\beta_{1-40}$ and the $A\beta_{1-40}$ mutant $A\beta_{40}$ -K16Nle which forms more stable aggregation intermediates [121].

On the other hand, the progress in the fibrillation process of $A\beta_{1-42}$ at nM concentrations was sensed according to the reduction of LSPR peak intensity of gold nano-urchins (AuNUs). With this method, the LSPR of AuNUs at 650 nm gradually decreased with time (Figure 8B) an effect that was also evident at various fibrillation stages of $A\beta_{1-42}$ (Figure 8B) [122]. In addition, $A\beta$ fibrillation at nM concentrations using AuNSps and AuNUs revealed that AuNSps did not show significant changes in optical absorption compared to AuNUs at various fibrillation stages (Figure 8B), thus limiting its capacity for sensing low concentrations in the fibrillation process.

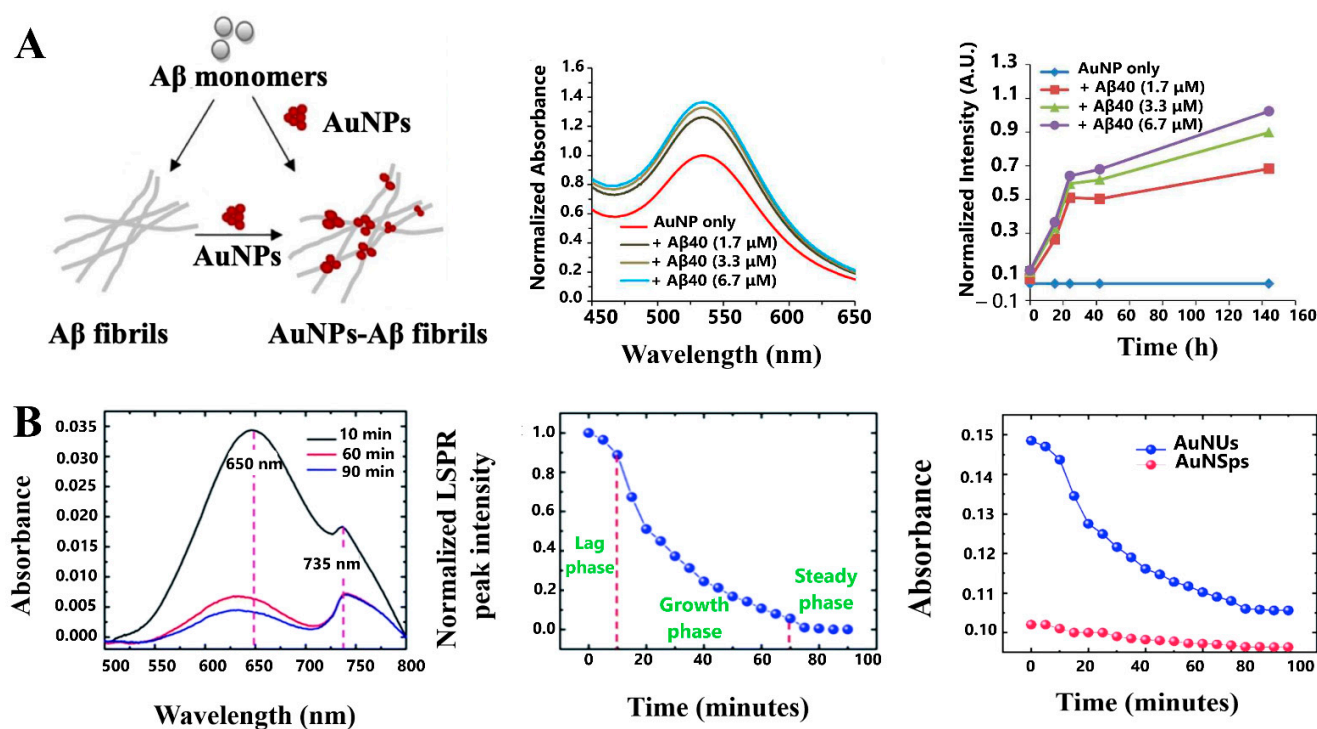


Figure 8. (A) $A\beta$ aggregation kinetics studies using AuNPs; UV-Vis spectra of AuNPs measured after 24 h of incubation and $A\beta_{1-40}$ aggregation kinetics followed by the LSPR band intensity change at 535 nm. Adapted with permission from ref. [121]. Copyright 2017 American Chemical Society. (B) Absorbance data of samples at 10, 60, and 90 min incubation times. The 650 nm and 735 nm absorbance peaks correspond to AuNUs and $A\beta$, respectively. LSPR sensing of various fibrillation stages of $A\beta_{1-42}$ and comparison between LSPR sensing of $A\beta$ fibrillation at nM range, using AuNUs (blue) and AuNSps (red). The three figures were obtained from ref. [122] published by The Royal Society of Chemistry.

Table 1 presents an overview of optical biosensors developed in the last decade for the detection of AD biomarkers.

Table 1. Overview of optical plasmonic sensors for in vitro detection of AD biomarkers.

Type of Nanoparticle	Detected Biomarker	Sensing Method	Analytical Parameters	Application	Ref.
Hybrid (MNPs/AuNPs)	tau	Antibody sandwich SERS assay	LR: 25 fM–500 nM LOD: <25 fM	-	[80]
AgNGSs	A β _{1–40} A β _{1–42}	Antibody sandwich SERS assay	LOD: 0.25 pg mL ^{−1} 0.33 pg mL ^{−1}	Human serum	[72]
MNPs@Au-HGO	A β _{1–42} tau	Antibody SERS assay	LOD: <100 fg mL ^{−1}	Blood	[83]
AuNPs	A β Os (A β _{1–42}) tau	Aptamer SERS detection	LOD: A β Os: 3.7 × 10 ^{−2} nM Tau: 4.2 × 10 ^{−4} pM	aCSF	[88]
AuNPs	A β _{1–42}	SERS detection with a fluorescent probe	L.R: 0–2 μ M	-	[78]
AuNPs	A β _{1–16} , A β _{1–40} , A β _{1–42} monomers	Colorimetric label-free detection	L.R: 0.2–5000 ng mL ^{−1} LOD: 40 pg mL ^{−1} (as total monomers)	CSF/AD rat brain tissues	[96]
AgNPs	A β _{1–40/1–42}	Colorimetric immunosensor	LR: 0.25–150 nM LOD: 86 pM	Blood	[100]
AuNPs	A β Os (A β _{1–40})	Colorimetric aptasensor	LR: 1–600 nM LOD: 0.56 nM	aCSF	[101]
AuNPs	miRNA-137	DNA based biosensor	LOD: 0.25 nM	Blood	[36]
AuNPs	Clusterin Fetuin B	Colorimetric microfluidic device	LOD: 0.24 nM 0.12 nM	-	[33]
AuNPs	A β Os	Fluorescence detection	LR: 0.1~1.0 nM LOD: 22.3 pM	-	[92]
AuNPs/CdTe QDs	A β Os	Fluorescence detection	LR: 1–60 nM LOD: 0.2–0.5 nM	-	[90]
AuNPs	A β _{1–42} Aggregates	Surface-Enhanced Fluorescence	μ M level	PBS	[93]
AuNRs	A β _{1–42} , A β _{1–40} , tau	Shape-code LSPR sensor	LR: 1 × 10 ¹ –1 × 10 ⁸ fM LOD: 26 fM	-	[107]
AuNPs	A β -tau complex	Antibody sandwich LSPR assay	LOD: 1 pM	CSF	[108]
AuNPs	A β _{1–42} Aggregates	LSPR sensor	LOD: 1.5 pM	aCSF	[105]

Abbreviations: LR: linear range, LOD: limit of detection, CSF: cerebrospinal fluid, aCSF: artificial cerebrospinal fluid, MNPs: magnetic nanoparticles, AuNPs: gold nanoparticles, AgNGSs: silver nano-gap shells, HGO: Hybrid graphene oxide, A β : Amyloid- β peptide, A β Os: Amyloid- β oligomers, CdTe QDs: Cadmium Telluride quantum dots, PBS: Phosphate-buffered saline.

5. In Vivo Imaging Detection Platforms of AD Using Plasmonic Nanoparticles

The definitive diagnosis of AD is only possible postmortem through neuropathological demonstration of A β plaques and NFTs. For this reason, the promise of “early diagnosis of AD” is the current focus in the development of diagnostic methods for imaging and molecular detection of biomarkers [123].

For brain imaging, the diagnostic modalities include positron emission tomography (PET), x-ray computed tomography (CT), and magnetic resonance imaging (MRI) [124]. Usually, after the appearance of the first clinical symptoms, the use of neuropsychological testing, in conjunction with these imaging techniques, allows one to estimate disease progression. Of the techniques mentioned above, PET and MRI have been the primary imaging modalities used in AD, which allow the assessment of cortical atrophy and amyloid load, respectively. Additionally, glucose metabolism has been measured using fluorodeoxyglucose-PET [125].

In PET, the compounds that have been used as probes for AD detection are the radiotracers (11)C-labeled Pittsburgh Compound-B (11)C-PiB, [18F] Flutemetamol, [18F] Florbetapir [126] that have been approved by the Food and Drug Administration (FDA). Despite this, they have not shown conclusive results as a precise diagnostic methodology

and are rather useful for monitoring the disease [126]. These radiotracers do not allow the detection of soluble A β species, so it would not be possible to make an early diagnosis, since they only detect insoluble A β species [126]. In addition, this technique has a great monetary cost, being necessary to have a nearby synchrotron to obtain the radiotracer. On the other hand, MRI provides excellent soft-tissue contrast and is considered safe because there is no need for ionizing radiation or radioactive traces at any point of the scanning process [124].

Due to the modifiable characteristics of NPs mentioned in Section 3 such as their size, shape, chemical composition, biocompatible coating, and the ability to be functionalized with a targeting ligand, fluorescent probe, or drug, render them as optimal candidates as contrast agents for imaging diagnostic applications in the central nervous system (CNS). For successful identification and imaging of plaques in AD, NPs-contrast agents must be able to cross the blood–brain barrier (BBB) [127]. Furthermore, these agents should maintain colloidal stability, safely interact with organs and display effective renal or hepatic clearance to prevent accumulation and toxic effects [125].

In literature has been reported that the NPs mostly used as contrast agents to improve sensitivity and enable the visualization of A β plaques by MRI are those that contain superparamagnetic (SPIONs) and magnetic iron cores (IONPs), which influence spin-spin (T₂, transversal) relaxation times of the protons present in water molecules in surrounding tissues. Chelates of Gadolinium (Gd), Gd³⁺ is usually available as standard T₁ (longitudinal) MRI contrast agents. In addition, the use of Gd-based small molecules [128,129] and Gd ions in NPs have been used in imaging applications [130,131]. More details about these contrast agents can be found in the interesting reviews by Ulanova et al. [125] and Sharma et al. [124].

In particular, studies regarding the use of plasmonic NPs for AD imaging are very limited. Some ex-vivo studies have been performed using AuNPs, with potential future applications in AD sensing [78,93,132]. However, a major disadvantage of these experiments is that they are not fully representative in antemortem conditions.

For in vivo imaging, in a literature search performed on PubMed databases using the following terms: Alzheimer's disease AND plasmonic nanoparticles AND in vivo imaging, only a few recent studies were found. Due to the fluorescence of AuNCs within the biological window, in 2016 Lai et al. developed a fluorescent method for in vivo imaging of the brain in an AD mouse model. Through the biosynthesis of AuNCs in brain affected sites with AD using an intravenous injection of a gold salt such as chloroauric acid (HAuCl₄), this method allowed the fluorescence labeling around these sites within a couple of hours, with a maximum at 18 h, compared to normal mouse brains (Figure 9A), which did not exhibit fluorescence. These results suggested that HAuCl₄ could pass the BBB and reach the brain of the AD mice, where it was observed that the accumulation of AuNCs was mainly in the hippocampus region as shown in Figure 9A [133].

Due to the high attenuation coefficient value of gold (5.16 cm² g⁻¹ at 100 keV), compared with contrast agents based on iodine (1.94 cm² g⁻¹ at 100 keV) [134], this element could be applied in imaging techniques such as CT. Perets et al. reported the use of intranasally administered exosomes from bone marrow mesenchymal stem cells (MSC-exo) labeled with AuNPs (MSC-exo-AuNPs). Using CT, this methodology allows the in vivo study of AD and other neurodegenerative, neurovascular, and neuropsychiatric diseases, such as Parkinson's disease (PD), ischemic stroke, and autism. In murine models, this technique allowed track of migration and homing patterns of the MSC-exo, revealing a selective accumulation in areas of the brain correlated with inflammatory mechanisms of these diseases (Figure 9B). Therefore, this system is an alternative to study the advancement of these types of diseases and anticipate more complex stages [135].

More recently, Yin et al. explored the potential of their 3D DNA walker nanoprobe (described in Section 4.2) for fluorescence imaging of A β O_s in the APP/PS1 double transgenic (Tg) AD mouse model, compared with C57BL/6 wild-type (WT) mice as controls. At all-time points from 30 to 360 min after injecting 2 nM of the nanoprobe, the fluorescence

signal in the brain was higher in Tg mice, compared to WT mice (Figure 9C), especially up to 240 min, and then rapidly decayed [92]. So, this nanosystem has great potential as a tool for AD diagnosis.

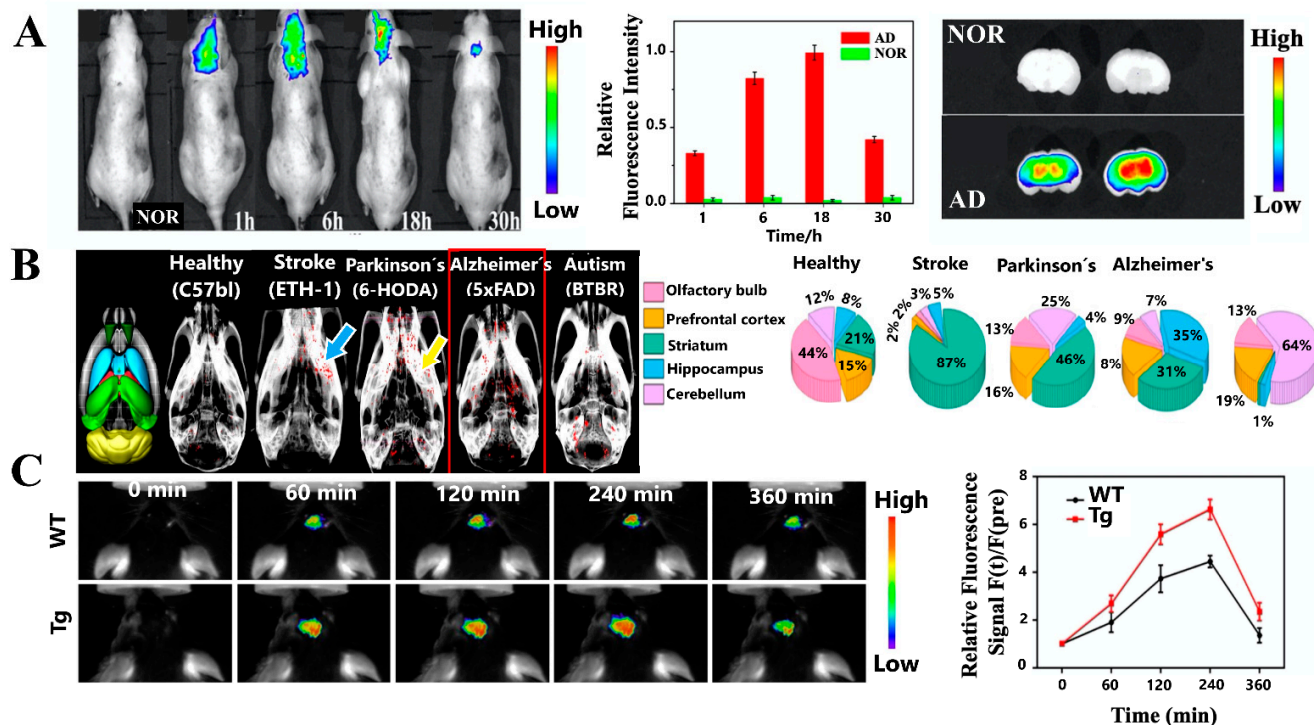


Figure 9. (A) Fluorescence imaging upon excitation at 420 nm of the blank control group (NOR) of mice and AD model mice via tail-vein injection of 10 mmol/L HAuCl₄ solution at 1 h, 6 h, 18 h, and 30 h. The variations of the relative fluorescence intensity in normal control mice and AD model mice indicate that at 18 h the maximum fluorescence intensity occurs. In a transverse section of NOR and AD mice's brain treated with 10 mmol/L HAuCl₄ solution at 30 h post-injection; no fluorescence signal was detected in the hippocampus of the NOR mice. Republished with permission of Royal Society of Chemistry, from ref. [133]. (B) In vivo CT imaging of AuNPs-loaded MSC-exo demonstrates different homing patterns in healthy controls, stroke, Parkinson's, Alzheimer's, and autism models, 24 h post intranasal administration. The light blue arrow indicates the location of the ETH-1 injection and the yellow arrow, the location of the 6-OHDA injection. Relevant brain sections were adapted from the Allen Mouse Brain 3D Atlas (dark green: olfactory bulb; blue: striatum; red: thalamus; green: hippocampus; and yellow: cerebellum). The percentage of the CT signal 96 h post-administration is shown for healthy control mice and stroke, Parkinson's disease, Alzheimer's disease, and autism models. Values are normalized to show percentiles, according to the total number of gold voxels in each brain. In AD model, the highest percentages of CT signal are found in the hippocampus and striatum regions. Reprinted with permission from ref. [135]. Copyright 2019 American Chemical Society. (C) In vivo fluorescence images and relative fluorescence signal of the WT (top row) and Tg (bottom row) mice at selected time points before and after injection of 3D DNA walker nanoprobes. Reprinted with permission from ref. [92]. Copyright 2020 American Chemical Society.

6. Conclusions and Perspectives

Due to the diagnosis of AD is made when irreversible brain damage has occurred, the development of cost-effective, non-invasive, portable, and rapid methods for the detection of AD biomarkers in the early stages and their discrimination from other types of dementia, play a key role for the timely treatment of this disease. In this aspect, the development of biosensors as powerful analytical devices seems necessary and unavoidable. Biosensors as analytical platforms allow highly sensitive and specific detection of a target analyte in a short period of time.

In this review, we have presented a summary of articles published in the last decade focused on the development of biosensors based on optical techniques incorporating

plasmonic nanoparticles for the *in vitro* detection of different biomarkers of AD, which the most common are the core biomarkers A β and tau protein.

Regarding this topic, four optical detection techniques (SERS, SEF, Colorimetry, and LSPR) were included because they mainly use plasmonic nanoparticles in their configuration. As mentioned in Section 3, these nanoparticles are very useful since they present the LSPR phenomena, which provides an increase in the local electromagnetic fields in the vicinity of the nanoparticles' surface and the optical extinction and scattering cross-sections [136]. This property, dependent on the chemical composition, size, shape, and medium in which the NPs are dispersed, allows increasing the signals in detection by SERS and SEF as well as observing color changes due to interaction of the nanoparticles with some analyte of interest or changes in the electromagnetic spectrum by displacement of the absorption bands of the NPs as in the LSPR-based sensors.

For the development of new sensing platforms, several key parameters must be considered. In this aspect, the World Health Organization (WHO), has defined seven parameters: "(i) Affordability, (ii) Sensitivity, (iii) Specificity, (iv) User-friendliness, (v) Rapid and robust, (vi) Equipment-free, and (vii) Deliverable to those in need for such technologies", defining the acronym "ASSURED" [137].

Of all sensor examples presented in this work, SERS and LSPR platforms are promising techniques that can reach LODs at femtomolar and picomolar concentration levels of an AD biomarker (A β peptide, tau protein). In the case of fluorescence and colorimetry detection, LOD are generally at the nanomolar range.

In general, SERS has great advantages as sensitivity, multiplexing capability, and resistance to photobleaching [138]. As described in Section 4, nominal parameters as enhancement factors and limits of detection are often used to compare the efficiency of a SERS sensor. However, currently, it has been reported that it cannot be considered as the only parameter when making a comparison [65]. In this regard, of the articles that report SERS sensors, the use of nanostructures type shells/core-shell and 3D superstructures are those that report the lowest detection limits (pg/mL and even fg/mL) and with enhancements factors in some cases of the order of 10^9 , however, in many of these works do not mention about other validation parameters, such as robustness, recovery, etc. Although this technique provides excellent sensitivity, the cost of the equipment, the need for qualified personnel to interpret results, are disadvantages that must be considered for a future clinical application. Currently, SERS-on-fiber technology can be a good alternative for obtaining portable platforms.

In the case of fluorescence-based sensing platforms using plasmonic nanoparticles, few articles have been reported in the detection of AD biomarkers, probably because most of these assays reach a sensitivity that is not clinically relevant [40]. Furthermore, it is necessary to design probes that allow an affinity for these biomarkers. One possibility could be the use of nanoparticles that present intrinsic fluorescence such as quantum dots (QDs) [139] which have some advantages compared to common fluorescent organic molecules, as tunable fluorescent wavelengths from the visible to red, high photostability [140], could be used in the development of biosensors and even in the field of imaging.

On the other hand, colorimetric techniques have the advantage of being low cost, simple and by the naked eye allows quantitative or semi-quantitative detection of a target analyte through a color change, but its main disadvantage is that it is generally less sensitive [141]. In the case of colorimetric platforms for AD biomarkers, many have limits of detection at the nanomolar level (nM) of concentration, which is not sufficient for clinical applications. It is interesting to note that unlike the other detection techniques presented in this review, colorimetric methods have been reported for sensing other less common AD biomarkers, such as miRNAs or Fetuin and Clusterin.

As the refractive index of metal nanoparticles depends on the size and shape, LSPR based-sensors can be useful since they have some advantages such as multiplexed detection, the possibility of miniaturization which reduces the sample volume to be used, and compatibility with microfluidics and *in flow* assays [44]. As a result, the LSPR detection

of AD biomarkers using plasmonic nanoparticles has allowed an ultrasensitive detection obtaining low detection limits of the order between pM and fM in some cases and has achieved the simultaneous detection of AD biomarkers such as A β and tau, so in the future, it is a technique that offers promising characteristics.

With respect to the type of matrix to be analyzed for the detection of AD biomarkers, to date, are commonly in CSF samples, since the fluid contains, in part, brain-derived proteins [25]. However, this is an invasive procedure since CSF analysis requires a lumbar puncture. To overcome these limitations, other biological fluids, such as blood, have been explored for the presence of detectable quantities of the A β peptide [25]. However, the use of blood samples remains a challenge because the difference in the level of blood-based A β between patients and normal individuals is very small (several 10 pg/mL) [142]. Although various methodologies have been developed to detect AD biomarkers in blood as A β , most of them have not achieved validate the clinical utility and have failed to replicate results [25,143]. In addition, for accurate detection of AD biomarkers in clinically relevant fluids generally requires recognition elements such as antibodies, aptamers, among others, which have high binding affinity and selectivity. Recently, the so-called nanobodies have emerged, an antigen-binding fragment with a small size, however, only some specific nanobodies for AD biomarkers detection have been reported [103,144].

It has been reported the development of portable optical sensing platforms [145–147]. Miniaturized platforms, as capillary, paper, and fiber-based would be very useful for AD detection due to their low cost, portability, and reduction of sample volume to be analyzed [141], which is important for a potential application in clinical diagnosis and multiplexed detection.

Although optical biosensors developed are still only appropriate for research purposes, transforming these platforms into robust practical tools continues to be another challenge. Apart from the advantages already described, the nanoparticles incorporated in these biosensors can be synthesized ensuring monodispersity in size and shape, as well as being stable against degradation and leaching. The possibility of reusing the sensor is another factor that must be considered for practical applications.

Another field that needs to be exploited is the study of the A β aggregation process. Currently, studies that use plasmonic NPs in this field are lacking, even though they can detect A β aggregates. Moreover, this type of NPs can determine which stage of the aggregation process is disrupted or sense. This information is valuable because several toxic species are formed in the protein aggregation process. Thus, the detection of these species would allow a rational design and development of a biosensor.

Unquestionably, AD diagnosis is possible only during a post-mortem examination of A β deposits and NFTs in the brain. Therefore, different diagnostic imaging techniques have been developed and used for observing neuroanatomical changes in AD. One of the most popular techniques to detect local brain functional changes is Positron Emission Tomography (PET). Magnetic Resonance Imaging (MRI) and X-ray computed tomography (CT), on the other hand, allow the assessment of structural changes in brain tissue. Even though they provide satisfying results, these methods are not completely specific and accurate. In this regard, the greatest challenge lies in the development of new tracers and contrast agents able to cross the blood-brain barrier (BBB) and reach the brain. This difficulty has been managed over the years by the use of nanotechnology, as mentioned in Section 5. In this section, we highlighted studies that used AuNPs to obtain a system that overcame the difficulty of reaching the brain, accumulated in areas of interest, and could be visualized by in vivo imaging techniques. These advances represent a great benefit for the research area as they allow expanding the field of diagnosis not only of AD, but also of other complex diseases with a difficult diagnosis. Furthermore, this knowledge has contributed to the generation of less harmful diagnostic systems than those used conventionally. Thus, the development of new nanosystems will allow to decrease the time of imaging taking, improve the quality of image acquisition, improved the information

acquired, and especially allow an early diagnosis, which could offer a better quality of life for people affected by AD.

Therefore, plasmonic-based platforms for AD diagnosis offer promising future features. In addition, multidisciplinary research is necessary to develop sensitive and reliable sensors that can be applied clinically and compete with those that are commercially available.

Finally, we encourage researchers to investigate the use of plasmonic NPs in detection methods for other kinds of AD biomarkers. Although there is a main focus on the A β peptide, other biomarkers such as tau protein, ApoE4, or miRNAs could also be used to complement AD diagnosis in the development of novel biosensors.

Author Contributions: Conceptualization, investigation, writing—original draft preparation, writing—review, and editing: M.P.O., A.T.-A., P.C. and P.J.-G.; supervision: M.J.K. All authors have read and agreed to the published version of the manuscript.

Funding: This research received no external funding.

Institutional Review Board Statement: Not Applicable.

Informed Consent Statement: Not Applicable.

Data Availability Statement: Not Applicable.

Acknowledgments: M. P. Oyarzún thanks Fondecyt Postdoctorate Project 3180651, A. Tapia-Arellano thanks Beca ANID 21151461 and 23190312, P. Cabrera thanks Beca Doctorado Nacional ANID 21200617, P. Jara-Guajardo thanks Beca Doctorado Nacional ANID 21180739, Fondecyt 1170929, and Fondap 15130011. The authors thank Eduardo Gallardo-Toledo for the elaboration of graphic content in this work (Figure 1 and Graphical abstract).

Conflicts of Interest: The authors declare no conflict of interest.

References

- Wenk, G.L. Neuropathologic changes in Alzheimer's disease. *J. Clin. Psychiatry* **2003**, *64*, 7–10. [[PubMed](#)]
- Ballard, C.; Gauthier, S.; Corbett, A.; Brayne, C.; Aarsland, D.; Jones, E. Alzheimer's disease. *Lancet* **2011**, *377*, 1019–1031. [[CrossRef](#)]
- Carneiro, P.; Morais, S.; Pereira, M.C. Nanomaterials towards biosensing of Alzheimer's disease biomarkers. *Nanomaterials* **2019**, *9*, 1663. [[CrossRef](#)]
- Karran, E.; Mercken, M.; De Strooper, B. The amyloid cascade hypothesis for Alzheimer's disease: An appraisal for the development of therapeutics. *Nat. Rev. Drug Discov.* **2011**, *10*, 698–712. [[CrossRef](#)] [[PubMed](#)]
- Selkoe, D.J.; Hardy, J. The amyloid hypothesis of Alzheimer's disease at 25 years. *EMBO Mol. Med.* **2016**, *8*, 595–608. [[CrossRef](#)] [[PubMed](#)]
- Knowles, T.P.; Vendruscolo, M.; Dobson, C.M. The amyloid state and its association with protein misfolding diseases. *Nat. Rev. Mol. Cell Biol.* **2014**, *15*, 384–396. [[CrossRef](#)] [[PubMed](#)]
- Chiti, F.; Dobson, C.M. Protein Misfolding, Amyloid Formation, and Human Disease: A Summary of Progress Over the Last Decade. *Annu. Rev. Biochem.* **2017**, *86*, 27–68. [[CrossRef](#)] [[PubMed](#)]
- Ameri, M.; Shabaninejad, Z.; Movahedpour, A.; Sahebkar, A.; Mohammadi, S.; Hosseindoost, S.; Ebrahimi, M.S.; Savardashtaki, A.; Karimipour, M.; Mirzaei, H. Biosensors for detection of Tau protein as an Alzheimer's disease marker. *Int. J. Biol. Macromol.* **2020**, *162*, 1100–1108. [[CrossRef](#)] [[PubMed](#)]
- Blennow, K.; Zetterberg, H.; Fagan, A.M. Fluid biomarkers in Alzheimer disease. *Cold Spring Harb. Perspect. Med.* **2012**, *2*, 1–24. [[CrossRef](#)] [[PubMed](#)]
- Rezabakhsh, A.; Rahbarghazi, R.; Fathi, F. Surface plasmon resonance biosensors for detection of Alzheimer's biomarkers; an effective step in early and accurate diagnosis. *Biosens. Bioelectron.* **2020**, *167*, 112511. [[CrossRef](#)]
- Bateman, R.J.; Xiong, C.; Benzinger, T.L.S.; Fagan, A.M.; Goate, A.; Fox, N.C.; Marcus, D.S.; Cairns, N.J.; Xie, X.; Blazey, T.M.; et al. Clinical and Biomarker Changes in Dominantly Inherited Alzheimer's Disease. *N. Engl. J. Med.* **2012**, *367*, 795–804. [[CrossRef](#)]
- Lehmann, S.; Delaby, C.; Boursier, G.; Cateau, C.; Ginestet, N.; Tiers, L.; Maceski, A.; Navucet, S.; Paquet, C.; Dumurgier, J.; et al. Relevance of A β 42/40 Ratio for Detection of Alzheimer Disease Pathology in Clinical Routine: The PLM(R) Scale. *Front. Aging Neurosci.* **2018**, *10*, 138. [[CrossRef](#)]
- Liu, C.C.; Kanekiyo, T.; Xu, H.; Bu, G. Apolipoprotein e and Alzheimer disease: Risk, mechanisms and therapy. *Nat. Rev. Neurol.* **2013**, *9*, 106–118. [[CrossRef](#)]
- Zhao, N.; Liu, C.C.; Qiao, W.; Bu, G. Apolipoprotein E, Receptors, and Modulation of Alzheimer's Disease. *Biol. Psychiatry* **2018**, *83*, 347–357. [[CrossRef](#)]

15. Carneiro, P.; Morais, S.; do Carmo Pereira, M. Biosensors on the road to early diagnostic and surveillance of Alzheimer's disease. *Talanta* **2020**, *211*, 120700. [[CrossRef](#)] [[PubMed](#)]
16. Anker, J.N.; Hall, W.P.; Lyandres, O.; Shah, N.C.; Zhao, J.; Duyn, R.P. Van Biosensing with plasmonic nanosensors. *Nat. Mater.* **2008**, *7*, 8–10. [[CrossRef](#)]
17. Jack, C.R.; Knopman, D.S.; Jagust, W.J.; Shaw, L.M.; Aisen, P.S.; Weiner, M.W.; Petersen, R.C.; Trojanowski, J.Q. Hypothetical model of dynamic biomarkers of the Alzheimer's pathological cascade. *Lancet Neurol.* **2010**, *9*, 119–128. [[CrossRef](#)]
18. Hardy, J.A.; Higgins, G.A. Science Alzheimer's disease: The amyloid cascade hypothesis. *Science* **1992**, *256*, 184–185. [[CrossRef](#)] [[PubMed](#)]
19. Klein, W.L.; Dis, J.A. Synaptotoxic amyloid- β oligomers: A molecular basis for the cause, diagnosis, and treatment of Alzheimer's disease? *J. Alzheimers Dis.* **2013**, *33*, S49–S65. [[CrossRef](#)]
20. Reinhard, C.; Hébert, S.S.; De Strooper, B. The amyloid-beta precursor protein: Integrating structure with biological function. *EMBO J.* **2005**, *24*, 3996–4006. [[CrossRef](#)]
21. Zheng, H.; Koo, E.H. The amyloid precursor protein: Beyond amyloid. *Mol. Neurodegener.* **2006**, *1*, 5. [[CrossRef](#)] [[PubMed](#)]
22. De Strooper, B.; Karran, E. The Cellular Phase of Alzheimer's Disease. *Cell* **2016**, *164*, 603–615. [[CrossRef](#)]
23. Cras, P.; Kawai, M.; Lowery, D.; Gonzalez-DeWhitt, P.; Greenberg, B.; Perry, G. Senile plaque neurites in Alzheimer disease accumulate amyloid precursor protein. *Proc. Natl. Acad. Sci. USA* **1991**, *88*, 7552–7556. [[CrossRef](#)]
24. Capetillo-Zarate, E.; Gracia, L.; Tampellini, D.; Gouras, G.K. Intraneuronal A β accumulation, amyloid plaques, and synapse pathology in Alzheimer's disease. *Neurodegener. Dis.* **2012**, *10*, 56–59. [[CrossRef](#)]
25. Veerabhadrapa, B.; Delaby, C.; Hirtz, C.; Vialaret, J.; Alcolea, D.; Lleó, A.; Fortea, J.; Santosh, M.S.; Choubey, S.; Lehmann, S. Detection of amyloid beta peptides in body fluids for the diagnosis of Alzheimer's disease: Where do we stand? *Crit. Rev. Clin. Lab. Sci.* **2020**, *57*, 99–113. [[CrossRef](#)]
26. Hansson, O.; Lehmann, S.; Otto, M.; Zetterberg, H.; Lewczuk, P. Advantages and disadvantages of the use of the CSF Amyloid β (A β) 42/40 ratio in the diagnosis of Alzheimer's Disease. *Alzheimers. Res. Ther.* **2019**, *11*, 34. [[CrossRef](#)] [[PubMed](#)]
27. Blennow, K.; Zetterberg, H.; Prog Mol Biol Transl, S. Fluid biomarker-based molecular phenotyping of Alzheimer's disease patients in research and clinical settings. *Prog. Mol. Biol. Transl. Sci.* **2019**, *169*, 3–23. [[CrossRef](#)]
28. Maeda, S.; Mucke, L. Previews Tau Phosphorylation—Much More than a Biomarker. *Neuron* **2016**, *92*, 265–267. [[CrossRef](#)]
29. Sunderland, T.; Linker, G.; Mirza, N.; Putnam, K.T.; Friedman, D.L.; Kimmel, L.H.; Bergeson, J.; Manetti, G.J.; Zimmermann, M.; Tang, B.; et al. Decreased β -Amyloid1-42 and Increased Tau Levels in Cerebrospinal Fluid of Patients with Alzheimer Disease. *J. Am. Med. Assoc.* **2003**, *289*, 2094–2103. [[CrossRef](#)]
30. Olsson, B.; Lautner, R.; Andreasson, U.; Öhrfelt, A.; Portelius, E.; Bjerke, M.; Hölttä, M.; Rosén, C.; Olsson, C. Articles CSF and blood biomarkers for the diagnosis of Alzheimer's disease: A systematic review and meta-analysis. *Lancet Neurol* **2016**, *15*, 673–684. [[CrossRef](#)]
31. Karikari, T.K.; Pascoal, T.A.; Ashton, N.J.; Janelidze, S.; Benedet, A.L.; Rodriguez, J.L.; Chamoun, M. Blood phosphorylated tau 181 as a biomarker for Alzheimer's disease: A diagnostic performance and prediction modelling study using data from four prospective cohorts. *Lancet Neurol.* **2020**, *19*, 422–433. [[CrossRef](#)]
32. Mantzavinos, V.; Alexiou, A. Biomarkers for Alzheimer's Disease Diagnosis. *Curr. Alzheimer Res.* **2017**, *14*, 1149–1154. [[CrossRef](#)]
33. Brazaca, L.C.; Moreto, J.R.; Martín, A.; Tehrani, F.; Wang, J.; Zucolotto, V. Colorimetric Paper-Based Immunosensor for Simultaneous Determination of Fetuin B and Clusterin toward Early Alzheimer's Diagnosis. *ACS Nano* **2019**, *13*, 13325–13332. [[CrossRef](#)] [[PubMed](#)]
34. Saunders, A.M. Apolipoprotein E and Alzheimer disease: An update on genetic and functional analyses. *J. Neuropathol. Exp. Neurol.* **2000**. [[CrossRef](#)]
35. Jonsson, T.; Atwal, J.K.; Steinberg, S.; Snaedal, J.; Jonsson, P.V.; Bjornsson, S.; Stefansson, H.; Sulem, P.; Gudbjartsson, D.; Maloney, J.; et al. A mutation in APP protects against Alzheimer's disease and age-related cognitive decline. *Nature* **2012**, *488*, 96–99. [[CrossRef](#)]
36. Delkhahi, S.; Rahaie, M.; Rahimi, F. Design and Fabrication a Gold Nanoparticle-DNA Based Nanobiosensor for Detection of microRNA Involved in Alzheimer's Disease. *J. Fluoresc.* **2017**, *27*, 603–610. [[CrossRef](#)]
37. Counts, S.E.; Ikonomic, M.D.; Mercado, N.; Vega, I.E.; Mufson, E.J. Biomarkers for the Early Detection and Progression of Alzheimer's Disease. *Neurotherapeutics* **2017**, *14*, 35–53. [[CrossRef](#)] [[PubMed](#)]
38. Blennow, K.; Zetterberg, H. Biomarkers for Alzheimer's disease: Current status and prospects for the future. *J. Intern. Med.* **2018**, *284*, 643–663. [[CrossRef](#)] [[PubMed](#)]
39. Cummings, J.L. Alzheimer's Disease. *N. Engl. J. Med.* **2004**, *351*, 56–67. [[CrossRef](#)] [[PubMed](#)]
40. Kim, K.; Lee, C.H.; Park, C.B. Chemical sensing platforms for detecting trace-level Alzheimer's core biomarkers. *Chem. Soc. Rev.* **2020**, *49*, 5446–5472. [[CrossRef](#)]
41. Willets, K.A.; Van Duyn, R.P. Localized Surface Plasmon Resonance Spectroscopy and Sensing. *Annu. Rev. Phys. Chem.* **2007**, *58*, 267–297. [[CrossRef](#)] [[PubMed](#)]
42. Krajczewski, J.; Kołataj, K.; Kudelski, A. Plasmonic nanoparticles in chemical analysis. *RSC Adv.* **2017**, *7*, 17559–17576. [[CrossRef](#)]
43. Elahi, N.; Kamali, M.; Baghersad, M.H. Recent biomedical applications of gold nanoparticles: A review. *Talanta* **2018**, *184*, 537–556. [[CrossRef](#)] [[PubMed](#)]

44. Sepúlveda, B.; Angelomé, P.C.; Lechuga, L.M.; Liz-Marzán, L.M. LSPR-based nanobiosensors. *Nano Today* **2009**, *4*, 244–251. [[CrossRef](#)]
45. Hu, M.; Chen, J.; Li, Z.Y.; Au, L.; Hartland, G.V.; Li, X.; Marquez, M.; Xia, Y. Gold nanostructures: Engineering their plasmonic properties for biomedical applications. *Chem. Soc. Rev.* **2006**, *35*, 1084–1094. [[CrossRef](#)]
46. Mie, G. Beiträge zur Optik trüber Medien, speziell kolloidaler Metallösungen. *Ann. Phys.* **1908**, *330*, 377–445. [[CrossRef](#)]
47. Gans, R. Über die Form ultramikroskopischer Goldteilchen. *Ann. Phys.* **1912**, *342*, 881–900. [[CrossRef](#)]
48. Nolan, J.P.; Sebba, D.S. *Surface-Enhanced Raman Scattering (SERS) Cytometry*, 2nd ed.; Elsevier Inc.: London, UK, 2011; Volume 102, ISBN 9780123749123.
49. Wang, L.; Hasanzadeh Kafshgari, M.; Meunier, M. Optical Properties and Applications of Plasmonic-Metal Nanoparticles. *Adv. Funct. Mater.* **2020**, *2005400*, 1–28. [[CrossRef](#)]
50. Young, J.K.; Figueroa, E.R.; Drezek, R.A. Tunable nanostructures as photothermal theranostic agents. *Ann. Biomed. Eng.* **2012**, *40*, 438–459. [[CrossRef](#)] [[PubMed](#)]
51. Indrasekara, A.S.D.S.; Thomas, R.; Fabris, L. Plasmonic properties of regiospecific core-satellite assemblies of gold nanostars and nanospheres. *Phys. Chem. Chem. Phys.* **2014**, *17*, 21133–21142. [[CrossRef](#)]
52. Bai, X.; Wang, Y.; Song, Z.; Feng, Y.; Chen, Y.; Zhang, D.; Feng, L. The basic properties of gold nanoparticles and their applications in tumor diagnosis and treatment. *Int. J. Mol. Sci.* **2020**, *21*, 2480. [[CrossRef](#)]
53. Polavarapu, L.; Pérez-Juste, J.; Xu, Q.H.; Liz-Marzán, L.M. Optical sensing of biological, chemical and ionic species through aggregation of plasmonic nanoparticles. *J. Mater. Chem. C* **2014**, *2*, 7460–7476. [[CrossRef](#)]
54. Mody, V.; Siwale, R.; Singh, A.; Mody, H. Introduction to metallic nanoparticles. *J. Pharm. Bioallied Sci.* **2010**, *2*, 282. [[CrossRef](#)]
55. Viswambari Devi, R.; Doble, M.; Verma, R.S. Nanomaterials for early detection of cancer biomarker with special emphasis on gold nanoparticles in immunoassays/sensors. *Biosens. Bioelectron.* **2015**, *68*, 688–698. [[CrossRef](#)]
56. Saeed, A.A.; Sánchez, J.L.A.; O’Sullivan, C.K.; Abbas, M.N. DNA biosensors based on gold nanoparticles-modified graphene oxide for the detection of breast cancer biomarkers for early diagnosis. *Bioelectrochemistry* **2017**, *118*, 91–99. [[CrossRef](#)]
57. Mieszawska, A.J.; Mulder, W.J.M.; Fayad, Z.A.; Cormode, D.P. Multifunctional gold nanoparticles for diagnosis and therapy of disease. *Mol. Pharm.* **2013**, *10*, 831–847. [[CrossRef](#)]
58. Mahan, M.M.; Doiron, A.L. Gold Nanoparticles as X-Ray, CT, and Multimodal Imaging Contrast Agents: Formulation, Targeting, and Methodology. *J. Nanomater.* **2018**, *2018*, 5837276. [[CrossRef](#)]
59. Ghosh, P.; Han, G.; De, M.; Kim, C.K.; Rotello, V.M. Gold nanoparticles in delivery applications. *Adv. Drug Deliv. Rev.* **2008**, *60*, 1307–1315. [[CrossRef](#)] [[PubMed](#)]
60. Farooq, M.U.; Novosad, V.; Rozhkova, E.A.; Wali, H.; Ali, A.; Fateh, A.A.; Neogi, P.B.; Neogi, A.; Wang, Z. Gold Nanoparticles-enabled Efficient Dual Delivery of Anticancer Therapeutics to HeLa Cells. *Sci. Rep.* **2018**, *8*, 2907. [[CrossRef](#)]
61. Arvizo, R.; Bhattacharya, R.; Mukherjee, P. Gold nanoparticles: Opportunities and challenges in nanomedicine. *Expert Opin. Drug Deliv.* **2010**, *7*, 753–763. [[CrossRef](#)]
62. Aghaie, T.; Jazayeri, M.H.; Manian, M.; Khani, I.; Erfani, M.; Rezayi, M.; Ferns, G.A.; Avan, A. Gold nanoparticle and polyethylene glycol in neural regeneration in the treatment of neurodegenerative diseases. *J. Cell. Biochem.* **2019**, *120*, 2749–2755. [[CrossRef](#)]
63. Credi, C.; Bibikova, O.; Dallari, C.; Tiribilli, B.; Ratto, F.; Centi, S.; Pini, R.; Artyushenko, V.; Cicchi, R.; Pavone, F.S. Fiber-cap biosensors for SERS analysis of liquid samples. *J. Mater. Chem. B* **2020**, *8*, 1629–1639. [[CrossRef](#)] [[PubMed](#)]
64. Wu, Y.; Tilley, R.D.; Gooding, J.J. Challenges and Solutions in Developing Ultrasensitive Biosensors. *J. Am. Chem. Soc.* **2019**, *141*, 1162–1170. [[CrossRef](#)] [[PubMed](#)]
65. Höller, R.P.M.; Jahn, I.J.; Cialla-May, D.; Chanana, M.; Popp, J.; Fery, A.; Kuttner, C. Biomacromolecular-Assembled Nanoclusters: Key Aspects for Robust Colloidal SERS Sensing. *ACS Appl. Mater. Interfaces* **2020**, *12*, 57302–57313. [[CrossRef](#)] [[PubMed](#)]
66. Zhang, Y.; Ren, B.; Zhang, D.; Liu, Y.; Zhang, M.; Zhao, C.; Zheng, J. Design principles and fundamental understanding of biosensors for amyloid- β detection. *J. Mater. Chem. B* **2020**, *8*, 6179–6196. [[CrossRef](#)]
67. McFarland, A.D.; Young, M.A.; Dieringer, J.A.; Van Duyne, R.P. Wavelength-Scanned Surface-Enhanced Raman Excitation Spectroscopy. *J. Phys. Chem. B* **2005**, *109*, 11279–11285. [[CrossRef](#)]
68. Sivapalan, S.T.; Devetter, B.M.; Yang, T.K.; Van Dijk, T.; Schulmerich, M.V.; Carney, P.S.; Bhargava, R.; Murphy, C.J. Off-resonance surface-enhanced raman spectroscopy from gold nanorod suspensions as a function of aspect ratio: Not what we thought. *ACS Nano* **2013**, *7*, 2099–2105. [[CrossRef](#)]
69. Höller, R.P.M.; Kuttner, C.; Mayer, M.; Wang, R.; Dulle, M.; Contreras-Cáceres, R.; Fery, A.; Liz-Marzán, L.M. Colloidal Superstructures with Triangular Cores: Size Effects on SERS Efficiency. *ACS Photonics* **2020**, *7*, 1839–1848. [[CrossRef](#)]
70. Kuttner, C.; Mayer, M.; Dulle, M.; Moscoso, A.; López-Romero, J.M.; Förster, S.; Fery, A.; Pérez-Juste, J.; Contreras-Cáceres, R. Seeded Growth Synthesis of Gold Nanotriangles: Size Control, SAXS Analysis, and SERS Performance. *ACS Appl. Mater. Interfaces* **2018**, *10*, 11152–11163. [[CrossRef](#)]
71. Kuttner, C. Plasmonics in Sensing: From Colorimetry to SERS Analytics. In *Plasmonics*; IntechOpen: London, UK, 2018; Chapter 9; ISBN 978-1-78984-435-1.
72. Yang, J.K.; Hwang, I.J.; Cha, M.G.; Kim, H.I.; Yim, D.B.; Jeong, D.H.; Lee, Y.S.; Kim, J.H. Reaction Kinetics-Mediated Control over Silver Nanogap Shells as Surface-Enhanced Raman Scattering Nanoprobes for Detection of Alzheimer’s Disease Biomarkers. *Small* **2019**, *15*, 1900613. [[CrossRef](#)]

73. El-Said, W.A.; Kim, T.H.; Yea, C.H.; Kim, H.; Choi, J.W. Fabrication of gold nanoparticle modified ITO substrate TO detect β -amyloid using surface-enhanced Raman scattering. *J. Nanosci. Nanotechnol.* **2011**, *11*, 768–772. [[CrossRef](#)] [[PubMed](#)]
74. Choi, I.; Huh, Y.S.; Erickson, D. Size-selective concentration and label-free characterization of protein aggregates using a Raman active nanofluidic device. *Lab Chip* **2011**, *11*, 632–638. [[CrossRef](#)] [[PubMed](#)]
75. Choi, I.; Suk, Y.; David, H. Ultra-sensitive, label-free probing of the conformational characteristics of amyloid beta aggregates with a SERS active nanofluidic device. *Microfluid. Nanofluid.* **2012**, *12*, 663–669. [[CrossRef](#)]
76. Dallari, C.; Credi, C.; Lenci, E.; Trabocchi, A.; Cicchi, R.; Pavone, F.S. Nanostars—decorated microfluidic sensors for surface enhanced Raman scattering targeting of biomolecules. *J. Phys. Photonics* **2020**, *2*, 024008. [[CrossRef](#)]
77. Lin, D.; Wu, Z.; Li, S.; Zhao, W.; Ma, C.; Wang, J.; Jiang, Z.; Zhong, Z.; Zheng, Y.; Yang, X. Large-Area Au-Nanoparticle-Functionalized Si Nanorod Arrays for Spatially Uniform Surface-Enhanced Raman Spectroscopy. *ACS Nano* **2017**, *11*, 1478–1487. [[CrossRef](#)]
78. Xia, Y.; Padmanabhan, P.; Sarangapani, S.; Gulyás, B.; Vadakke Matham, M. Bifunctional Fluorescent/Raman Nanoprobe for the Early Detection of Amyloid. *Sci. Rep.* **2019**, *9*, 1–11. [[CrossRef](#)]
79. Billings, L.M.; Oddo, S.; Green, K.N.; McLaugh, J.L.; LaFerla, F.M. Intraneuronal A β Causes the Onset of Early Alzheimer’s Disease-Related Cognitive Deficits in Transgenic Mice. *Neuron* **2005**, *45*, 675–688. [[CrossRef](#)] [[PubMed](#)]
80. Zengin, A.; Tamer, U.; Caykara, T. A SERS-based sandwich assay for ultrasensitive and selective detection of Alzheimer’s tau protein. *Biomacromolecules* **2013**, *14*, 3001–3009. [[CrossRef](#)]
81. Maurer, V.; Frank, C.; Porsiel, J.C.; Zellmer, S.; Garnweitner, G.; Stosch, R. Step-by-step monitoring of a magnetic and SERS-active immunosensor assembly for purification and detection of tau protein. *J. Biophotonics* **2020**, *13*, e201960090. [[CrossRef](#)]
82. Sinha, S.S.; Jones, S.; Pramanik, A.; Ray, P.C. Nanoarchitecture Based SERS for Biomolecular Fingerprinting and Label-Free Disease Markers Diagnosis. *Acc. Chem. Res.* **2016**, *49*, 2725–2735. [[CrossRef](#)]
83. Demeritte, T.; Priya, B.; Nellore, V.; Kanchanapally, R.; Sinha, S.S.; Pramanik, A.; Chavva, S.R.; Ray, P.C. Hybrid Graphene Oxide Based Plasmonic-Magnetic Multifunctional Nanoplatfor m for Selective Separation and Label-Free Identification of Alzheimer’s Disease Biomarkers. *ACS Appl. Mater. Interfaces* **2015**, *7*, 13693–13700. [[CrossRef](#)]
84. Rodrigues, D.C.; Andrade, G.F.S.; Temperini, M.L.A. SERS performance of gold nanotubes obtained by sputtering onto polycarbonate track-etched membranes. *Phys. Chem. Chem. Phys.* **2013**, *15*, 1169–1176. [[CrossRef](#)] [[PubMed](#)]
85. Scarabelli, L.; Coronado-Puchau, M.; Giner-Casares, J.J.; Langer, J.; Liz-Marzán, L.M. Monodisperse gold nanotriangles: Size control, large-scale self-assembly, and performance in surface-enhanced raman scattering. *ACS Nano* **2014**, *8*, 5833–5842. [[CrossRef](#)] [[PubMed](#)]
86. Park, H.J.; Cho, S.; Kim, M.; Jung, Y.S. Carboxylic Acid-Functionalized, Graphitic Layer-Coated Three-Dimensional SERS Substrate for Label-Free Analysis of Alzheimer’s Disease Biomarkers. *Nano Lett.* **2020**, *20*, 2576–2584. [[CrossRef](#)]
87. Pei, H.; Li, F.; Wan, Y.; Wei, M.; Liu, H.; Su, Y.; Chen, N.; Huang, Q.; Fan, C. Designed Diblock Oligonucleotide for the Synthesis of Spatially Isolated and Highly Hybridizable Functionalization of DNA–Gold Nanoparticle Nanoconjugates. *J. Am. Chem. Soc.* **2012**, *134*, 11876–11879. [[CrossRef](#)] [[PubMed](#)]
88. Zhang, X.; Liu, S.; Song, X.; Wang, H.; Wang, J.; Wang, Y.; Huang, J.; Yu, J. Robust and Universal SERS Sensing Platform for Multiplexed Detection of Alzheimer’s Disease Core Biomarkers Using PAapt-AuNPs Conjugates. *ACS Sens.* **2019**, *4*, 2140–2149. [[CrossRef](#)]
89. Carlomagno, C.; Cabinio, M.; Picciolini, S.; Gualerzi, A.; Baglio, F.; Bedoni, M. SERS-based biosensor for Alzheimer disease evaluation through the fast analysis of human serum. *J. Biophotonics* **2020**, *13*, e201960033. [[CrossRef](#)]
90. Xia, N.; Zhou, B.; Huang, N.; Jiang, M.; Zhang, J.; Liu, L. Visual and fluorescent assays for selective detection of beta-amyloid oligomers based on the inner filter effect of gold nanoparticles on the fluorescence of CdTe quantum dots. *Biosens. Bioelectron.* **2016**, *85*, 625–632. [[CrossRef](#)]
91. Saini, M.; Sadhu, K.K. Two instantaneous fluorogenic steps for detection of nanomolar amyloid beta monomer and its interaction with stoichiometric copper(II) ion. *Sens. Actuators B Chem.* **2020**, *303*, 127086. [[CrossRef](#)]
92. Yin, Y.; Chen, G.; Gong, L.; Ge, K.; Pan, W.; Li, N.; Machuki, J.O.; Yu, Y.; Geng, D.; Dong, H.; et al. DNAzyme-Powered Three-Dimensional DNA Walker Nanoprobe for Detection Amyloid β -Peptide Oligomer in Living Cells and in Vivo. *Anal. Chem.* **2020**, *92*, 9247–9256. [[CrossRef](#)]
93. Jara-Guajardo, P.; Cabrera, P.; Celis, F.; Soler, M.; Berlanga, I.; Parra-Muñoz, N.; Acosta, G.; Albericio, F.; Guzman, F.; Campos, M.; et al. Gold nanoparticles mediate improved detection of β -amyloid aggregates by fluorescence. *Nanomaterials* **2020**, *10*, 690. [[CrossRef](#)] [[PubMed](#)]
94. Han, X.; Man, Z.; Xu, S.; Cong, L.; Wang, Y.; Wang, X.; Du, Y.; Zhang, Q.; Tang, S.; Liu, Z.; et al. A gold nanocluster chemical tongue sensor array for Alzheimer’s disease diagnosis. *Colloids Surf. B Biointerfaces* **2019**, *173*, 478–485. [[CrossRef](#)] [[PubMed](#)]
95. Chang, C.C.; Chen, C.P.; Wu, T.H.; Yang, C.H.; Lin, C.W.; Chen, C.Y. Gold nanoparticle-based colorimetric strategies for chemical and biological sensing applications. *Nanomaterials* **2019**, *9*, 861. [[CrossRef](#)]
96. Yu, Y.; Zhang, L.; Sun, X.; Li, C.; Qiu, Y.; Sun, H.; Tang, D.; Liu, Y.; Yin, X. A sensitive colorimetric strategy for monitoring cerebral β -amyloid peptides in AD based on dual-functionalized gold nanoplasmonic particles. *Chem. Commun.* **2015**, *51*, 8880–8883. [[CrossRef](#)]
97. Zhou, Y.; Dong, H.; Liu, L.; Xu, M. Simple colorimetric detection of amyloid β -peptide (1–40) based on aggregation of gold nanoparticles in the presence of copper ions. *Small* **2015**, *11*, 2144–2149. [[CrossRef](#)]

98. Ghasemi, F.; Reza Hormozi-Nezhad, M.; Mahmoudi, M. Label-free detection of β -amyloid peptides ($A\beta_{40}$ and $A\beta_{42}$): A colorimetric sensor array for plasma monitoring of Alzheimer's disease. *Nanoscale* **2018**, *10*, 6361–6368. [[CrossRef](#)]
99. Hu, T.; Lu, S.; Chen, C.; Sun, J.; Yang, X. Colorimetric sandwich immunosensor for $A\beta(1-42)$ based on dual antibody-modified gold nanoparticles. *Sens. Actuators B Chem.* **2017**, *243*, 792–799. [[CrossRef](#)]
100. Hu, T.; Chen, C.; Huang, G.; Yang, X. Antibody modified-silver nanoparticles for colorimetric immuno sensing of $A\beta(1-40/1-42)$ based on the interaction between β -amyloid and Cu^{2+} . *Sens. Actuators B Chem.* **2016**, *234*, 63–69. [[CrossRef](#)]
101. Zhu, X.; Zhang, N.; Zhang, Y.; Liu, B.; Chang, Z.; Zhou, Y.; Hao, Y.; Ye, B.; Xu, M. A sensitive gold nanoparticle-based aptasensor for colorimetric detection of $A\beta_{1-40}$ oligomers. *Anal. Methods* **2018**, *10*, 641–645. [[CrossRef](#)]
102. Li, M.; Guan, Y.; Zhao, A.; Ren, J.; Qu, X. Using multifunctional peptide conjugated Au nanorods for monitoring β -amyloid aggregation and chemo-photothermal treatment of Alzheimer's disease. *Theranostics* **2017**, *7*, 2996–3006. [[CrossRef](#)]
103. Ren, X.; Yan, J.; Wu, D.; Wei, Q.; Wan, Y. Nanobody-Based Apolipoprotein E Immunosensor for Point-of-Care Testing. *ACS Sens.* **2017**, *2*, 1267–1271. [[CrossRef](#)] [[PubMed](#)]
104. Haes, A.J.; Chang, L.; Klein, W.L.; Van Duyne, R.P. Detection of a biomarker for Alzheimer's disease from synthetic and clinical samples using a nanoscale optical biosensor. *J. Am. Chem. Soc.* **2005**, *127*, 2264–2271. [[CrossRef](#)]
105. Kang, M.K.; Lee, J.; Nguyen, A.H.; Sim, S.J. Label-free detection of ApoE4-mediated β -amyloid aggregation on single nanoparticle uncovering Alzheimer's disease. *Biosens. Bioelectron.* **2015**, *72*, 197–204. [[CrossRef](#)] [[PubMed](#)]
106. Kim, H.; Lee, J.U.; Kim, S.; Song, S.; Sim, S.J. A Nanoplasmonic Biosensor for Ultrasensitive Detection of Alzheimer's Disease Biomarker Using a Chaotropic Agent. *ACS Sens.* **2019**, *4*, 595–602. [[CrossRef](#)] [[PubMed](#)]
107. Kim, H.; Lee, J.U.; Song, S.; Kim, S.; Sim, S.J. A shape-code nanoplasmonic biosensor for multiplex detection of Alzheimer's disease biomarkers. *Biosens. Bioelectron.* **2018**, *101*, 96–102. [[CrossRef](#)] [[PubMed](#)]
108. Špringer, T.; Hemmerová, E.; Finocchiaro, G.; Křištofiková, Z.; Vyhánek, M.; Homola, J. Surface plasmon resonance biosensor for the detection of tau-amyloid β complex. *Sens. Actuators B Chem.* **2020**, *316*. [[CrossRef](#)]
109. Stefani, M.; Dobson, C.M. Protein aggregation and aggregate toxicity: New insights into protein folding, misfolding diseases and biological evolution. *J. Mol. Med.* **2003**, *81*, 678–699. [[CrossRef](#)]
110. Ross, C.A.; Poirier, M.A. Protein aggregation and neurodegenerative disease. *Nat. Med.* **2004**, *10* (Suppl. S10–S17). [[CrossRef](#)]
111. Dobson, C.M. The structural basis of protein folding and its links with human disease. *Philos. Trans. R. Soc. Lond. B Biol. Sci.* **2001**, *356*, 133–145. [[CrossRef](#)]
112. Chiti, F.; Dobson, C.M. Protein misfolding, functional amyloid, and human disease. *Annu. Rev. Biochem.* **2006**, *75*, 333–366. [[CrossRef](#)] [[PubMed](#)]
113. Sengupta, U.; Nilson, A.N.; Kaye, R. The Role of Amyloid- β Oligomers in Toxicity, Propagation, and Immunotherapy. *EBioMedicine* **2016**, *6*, 42–49. [[CrossRef](#)]
114. Serra-Batiste, M.; Ninot-Pedrosa, M.; Bayoumi, M.; Gairí, M.; Maglia, G.; Carulla, N. $A\beta_{42}$ assembles into specific β -barrel pore-forming oligomers in membrane-mimicking environments. *Proc. Natl. Acad. Sci. USA* **2016**, *113*, 10866–10871. [[CrossRef](#)] [[PubMed](#)]
115. Ahmed, M.; Davis, J.; Aucoin, D.; Sato, T.; Ahuja, S.; Aimoto, S.; Elliott, J.I.; Van Nostrand, W.E.; Smith, S.O. Structural conversion of neurotoxic amyloid-beta(1-42) oligomers to fibrils. *Nat. Struct. Mol. Biol.* **2010**, *17*, 561–567. [[CrossRef](#)]
116. Arosio, P.; Vendruscolo, M.; Dobson, C.M.; Knowles, T.P. Chemical kinetics for drug discovery to combat protein aggregation diseases. *Trends Pharmacol. Sci.* **2014**, *35*, 127–135. [[CrossRef](#)] [[PubMed](#)]
117. Arosio, P.; Knowles, T.P.; Linse, S. On the lag phase in amyloid fibril formation. *Phys. Chem. Chem. Phys.* **2015**, *17*, 7606–7618. [[CrossRef](#)]
118. Arosio, P.; Michaels, T.C.; Linse, S.; Månsson, C.; Emanuelsson, C.; Presto, J.; Johansson, J.; Vendruscolo, M.; Dobson, C.M.; Knowles, T.P. Kinetic analysis reveals the diversity of microscopic mechanisms through which molecular chaperones suppress amyloid formation. *Nat. Commun.* **2016**, *7*, 10948. [[CrossRef](#)]
119. Hellstrand, E.; Boland, B.; Walsh, D.M.; Linse, S. Amyloid β -protein aggregation produces highly reproducible kinetic data and occurs by a two-phase process. *ACS Chem. Neurosci.* **2010**, *1*, 13–18. [[CrossRef](#)]
120. Novo, M.; Freire, S.; Al-Soufi, W. Critical aggregation concentration for the formation of early Amyloid- β (1-42) oligomers. *Sci. Rep.* **2018**. [[CrossRef](#)] [[PubMed](#)]
121. Elbassal, E.A.; Morris, C.; Kent, T.W.; Lantz, R.; Ojha, B.; Wojcikiewicz, E.P.; Du, D. Gold Nanoparticles as a Probe for Amyloid- β Oligomer and Amyloid Formation. *J. Phys. Chem. C* **2017**, *121*, 20007–20015. [[CrossRef](#)] [[PubMed](#)]
122. Nair, R.V.; Yi, P.J.; Padmanabhan, P.; Gulyás, B.; Murukeshan, V.M. Au nano-urchins enabled localized surface plasmon resonance sensing of beta amyloid fibrillation. *Nanoscale Adv.* **2020**. [[CrossRef](#)]
123. Ahmad, J.; Akhter, S.; Rizwanullah, M.; Khan, M.A.; Pigeon, L.; Addo, R.T.; Greig, N.H.; Midoux, P.; Pichon, C.; Kamal, M.A. Nanotechnology Based Theranostic Approaches in Alzheimer's Disease Management: Current Status and Future Perspective. *Curr. Alzheimer Res.* **2017**, *14*, 1164–1181. [[CrossRef](#)]
124. Sharma, B.; Pervushin, K. Magnetic nanoparticles as in vivo tracers for alzheimer's disease. *Magnetochemistry* **2020**, *6*, 13. [[CrossRef](#)]
125. Ulanova, M.; Poljak, A.; Wen, W.; Bongers, A.; Gloag, L.; Gooding, J.; Tilley, R.; Sachdev, P.; Braidy, N. Nanoparticles as contrast agents for the diagnosis of Alzheimer's disease: A systematic review. *Nanomedicine* **2020**, *15*, 725–743. [[CrossRef](#)]

126. Pietrzak, K.; Czarnecka, K.; Mikiciuk-Olasik, E.; Szymanski, P. New Perspectives of Alzheimer Disease Diagnosis—The Most Popular and Future Methods. *Med. Chem.* **2018**, *14*, 34–43. [[CrossRef](#)]
127. Ajetunmobi, A.; Prina-Mello, A.; Volkov, Y.; Corvin, A.; Tropea, D. Nanotechnologies for the study of the central nervous system. *Prog. Neurobiol.* **2014**, *123*, 18–36. [[CrossRef](#)] [[PubMed](#)]
128. Tanifum, E.A.; Ghaghada, K.; Vollert, C.; Head, E.; Eriksen, J.L.; Annapragada, A. A Novel Liposomal Nanoparticle for the Imaging of Amyloid Plaque by Magnetic Resonance Imaging. *J. Alzheimers. Dis.* **2016**, *52*, 731–745. [[CrossRef](#)]
129. Badachhape, A.A.; Working, P.K.; Srivastava, M.; Bhandari, P.; Stupin, I.V.; Devkota, L.; Tanifum, E.A.; Annapragada, A.V.; Ghaghada, K.B. Pre-clinical dose-ranging efficacy, pharmacokinetics, tissue biodistribution, and toxicity of a targeted contrast agent for MRI of amyloid deposition in Alzheimer’s disease. *Sci. Rep.* **2020**, *10*, 16185. [[CrossRef](#)] [[PubMed](#)]
130. Aouidat, F.; Boumati, S.; Khan, M.; Tielens, F.; Doan, B.T.; Spadavecchia, J. Design and synthesis of gold-gadolinium-coreshell nanoparticles as contrast agent: A smart way to future nanomaterials for nanomedicine applications. *Int. J. Nanomed.* **2019**, *14*, 9309–9324. [[CrossRef](#)]
131. Faucher, L.; Tremblay, M.; Lagueux, J.; Gossuin, Y.; Fortin, M.-A. Rapid Synthesis of PEGylated Ultrasmall Gadolinium Oxide Nanoparticles for Cell Labeling and Tracking with MRI. *ACS Appl. Mater. Interfaces* **2012**, *4*, 4506–4515. [[CrossRef](#)]
132. Guerrero, S.; Araya, E.; Fiedler, J.L.; Arias, J.I.; Adura, C.; Albericio, F.; Giralt, E.; Arias, J.L.; Fernandez, M.S.; Kogan, M.J. Improving the brain delivery of gold nanoparticles by conjugation with an amphipathic peptide. *Nanomedicine* **2010**, *5*, 897–913. [[CrossRef](#)]
133. Lai, L.; Zhao, C.; Li, X.; Liu, X.; Jiang, H.; Selke, M.; Wang, X. Fluorescent gold nanoclusters for in vivo target imaging of Alzheimer’s disease. *RSC Adv.* **2016**, *6*, 30081–30088. [[CrossRef](#)]
134. Han, X.; Xu, K.; Taratula, O.; Farsad, K. Applications of nanoparticles in biomedical imaging. *Nanoscale* **2019**, *11*, 799–819. [[CrossRef](#)]
135. Perets, N.; Betzer, O.; Shapira, R.; Brenstein, S.; Angel, A.; Sadan, T.; Ashery, U.; Popovtzer, R.; Offen, D. Golden Exosomes Selectively Target Brain Pathologies in Neurodegenerative and Neurodevelopmental Disorders. *Nano Lett.* **2019**, *19*, 3422–3431. [[CrossRef](#)]
136. Szunerits, S.; Boukherroub, R. Sensing using localised surface plasmon resonance sensors. *Chem. Commun.* **2012**, *48*, 8999–9010. [[CrossRef](#)] [[PubMed](#)]
137. Hosseini, S.; Vázquez-Villegas, P.; Rito-Palomares, M.; Martínez-Chapa, S.O. (Eds.) *Advantages, Disadvantages and Modifications of Conventional ELISA BT—Enzyme-Linked Immunosorbent Assay (ELISA): From A to Z*; Springer: Singapore, 2018; pp. 67–115, ISBN 978-981-10-6766-2.
138. Kang, H.; Jeong, S.; Yang, J.K.; Jo, A.; Lee, H.; Heo, E.H.; Jeong, D.H.; Jun, B.H.; Chang, H.; Lee, Y.S. Template-assisted plasmonic nanogap shells for highly enhanced detection of cancer biomarkers. *Int. J. Mol. Sci.* **2021**, *22*, 1752. [[CrossRef](#)]
139. Quan, L.; Wu, J.; Lane, L.A.; Wang, J.; Lu, Q.; Gu, Z.; Wang, Y. Enhanced Detection Specificity and Sensitivity of Alzheimer’s Disease Using Amyloid- β -Targeted Quantum Dots. *Bioconjug. Chem.* **2016**, *27*, 809–814. [[CrossRef](#)]
140. Hong, S.; Lee, C. The current status and future outlook of quantum dot-based biosensors for plant virus detection. *Plant Pathol. J.* **2018**, *34*, 85–92. [[CrossRef](#)]
141. Mirsalari, M.; Elhami, S. Colorimetric detection of insulin in human serum using GO/AuNPs/TX-100 nanocomposite. *Spectrochim. Acta Part A Mol. Biomol. Spectrosc.* **2020**, *240*, 118617. [[CrossRef](#)]
142. Yoo, Y.K.; Kim, G.; Park, D.; Kim, J.; Kim, Y.; Yun Kim, H.; Yang, S.H.; Lee, J.H.; Hwang, K.S. Gold nanoparticles assisted sensitivity improvement of interdigitated microelectrodes biosensor for amyloid- β detection in plasma sample. *Sens. Actuators B Chem.* **2020**, *308*, 127710. [[CrossRef](#)]
143. Altuna-Azkargorta, M.; Mendioroz-Iriarte, M. Blood biomarkers in Alzheimer’s disease. *Neurología* **2020**. In Press. [[CrossRef](#)]
144. Kasturirangan, S.; Li, L.; Emadi, S.; Boddapati, S.; Schulz, P.; Sierks, M.R. Nanobody specific for oligomeric beta-amyloid stabilizes nontoxic form. *Neurobiol. Aging* **2012**, *33*, 1320–1328. [[CrossRef](#)]
145. Lertvachirapaiboon, C.; Baba, A.; Shinbo, K.; Kato, K. A smartphone-based surface plasmon resonance platform. *Anal. Methods* **2018**, *10*, 4732–4740. [[CrossRef](#)]
146. Zeng, F.; Duan, W.; Zhu, B.; Mu, T.; Zhu, L.; Guo, J.; Ma, X. Paper-Based Versatile Surface-Enhanced Raman Spectroscopy Chip with Smartphone-Based Raman Analyzer for Point-of-Care Application. *Anal. Chem.* **2019**, *91*, 1064–1070. [[CrossRef](#)]
147. Zeng, F.; Mou, T.; Zhang, C.; Huang, X.; Wang, B.; Ma, X.; Guo, J. Paper-based SERS analysis with smartphones as Raman spectral analyzers. *Analyst* **2019**, *144*, 137–142. [[CrossRef](#)]